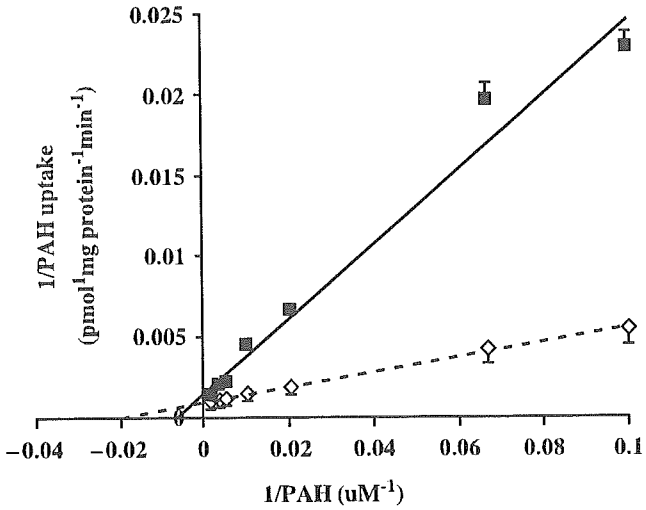

Fig. 4. Kinetic analysis of steviol inhibition. The S2 cells expressing hOAT1 were incubated with D-PBS containing [^{14}C]-PAH at concentrations from 10 to 600 μM in the absence (◇) or presence (■) of steviol (20 μM). Data are shown as the reciprocal of PAH uptake on the ordinate *vs.* the reciprocal of PAH concentrations in the medium on the abscissa. The data shown are from a representative experiment.

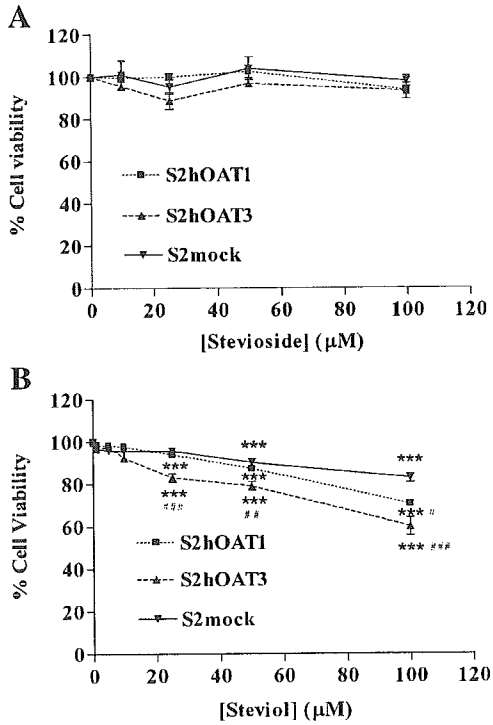

Fig. 5. Effects of stevioside (A) and steviol (B) on cell viability. The S2 cells expressing hOAT1, hOAT3, and S2mock were subcultivated in 96-well plates with various concentrations of either stevioside or steviol. The cell viability of S2hOAT1 (■), S2hOAT3 (▲), and S2mock (▼) were measured after 3 days of incubation. Each point represents the percentage of cell viability in the absence of either stevioside or steviol (mean ± SE) of three separate experiments. $^{*}p < 0.05$, $^{**}p < 0.01$, $^{***}p < 0.001$ *vs.* control; whereas $^{\#}p < 0.05$, $^{\#\#}p < 0.01$, $^{\#\#\#}p < 0.001$ *vs.* S2mock cells.

mg protein^{-1} min^{-1}), suggesting competitive inhibition. The calculated K_i of steviol on PAH uptake mediated by hOAT1 was 8.2 μM.

Effect of Stevioside and Steviol on Cell Viability

We examined cell viability after exposure to stevioside and steviol. As shown in Fig. 5A, stevioside in the range between 1 and 100 μM did not affect the cell viability of S2hOAT1, S2hOAT3, and S2mock cells. At 1 to 10 μM, steviol did not affect cell viability in S2hOAT1, S2hOAT3, or S2mock cells, but at concentrations from 25 to 100 μM, steviol reduced the cell viability of all cell types, with the greatest suppression observed in the hOAT1 and hOAT3 expressing cells (Fig. 5B). Steviol at concentrations from 25 to 100 μM significantly decreased the cell viability in S2hOAT3, whereas only 100 μM steviol significantly reduced cell viability in S2hOAT1. In addition, as a positive control, the effects of a cytotoxic drug, methotrexate, on S2hOAT1, S2hOAT3, and S2mock were examined. Methotrexate at a

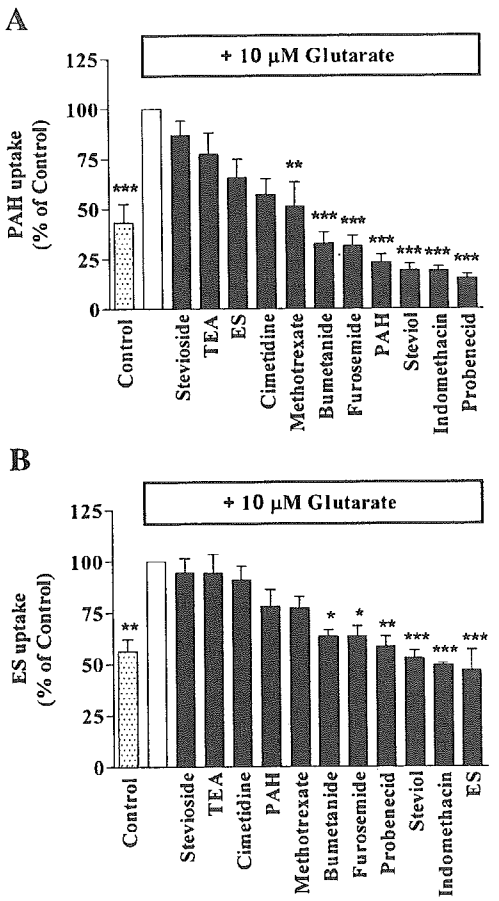

Fig. 6. The relative inhibition of stevioside, steviol, and various compounds on PAH (A) and ES (B) transport in mouse renal cortical slices. The fresh renal slices were incubated in the medium containing 10 μM of [^{3}H]-PAH and 100 nM of [^{3}H]-ES with or without 100 μM of compounds for 60 min at room temperature. The data are calculated as tissue/medium ratio and expressed as a mean percentage of control uptake (mean ± SE) of three separate experiments. Mean control T/M ratios were 8.3 ± 1.3 (PAH) and 16.1 ± 1.7 (ES), respectively. Each experiment used three to five animals. $^{*}p < 0.05$, $^{**}p < 0.01$, $^{***}p < 0.001$ *vs.* control.

very low concentration, 1 μM, killed all S2hOAT1 cells. It was less toxic to S2hOAT3 and S2mock cells, showing 25% and 60% cell viability, respectively (data not shown).

Mouse Renal Cortical Slices

The data presented above indicate that in hOAT1 and hOAT3 expressing cell lines, steviol was an effective inhibitor, whereas stevioside was not. To assess whether these same properties are expressed in an intact renal epithelium, the effects of both agents were determined in mouse renal cortical slices. PAH is a substrate for both OAT1 and OAT3 in mouse (27), so its uptake by the mouse slice reflects the action of both carriers. As shown in Fig. 6A, control PAH uptake in renal cortical slice was increased when 10 μM glutarate was added to the medium, as previously reported (28). Therefore, 10 μM glutarate was applied in all renal cortical slice experiments. The presence of 100 μM methotrexate, bumetanide, furosemide, unlabeled PAH, steviol, indomethacin, and probenecid significantly decreased PAH uptake, whereas stevioside, TEA, unlabeled ES, and cimetidine did not affect PAH uptake by mouse renal cortical slices. To examine the effects of stevioside and steviol on the mouse OAT3 specifically, the uptake of ES was assessed, as this substrate is only transported across the basolateral membrane of the proximal tubule via OAT3 (27). As shown in Fig. 6B, the presence of 100 μM bumetanide, furosemide, probenecid, steviol, indomethacin, and unlabeled ES inhibited ES uptake, whereas stevioside, TEA, cimetidine, unlabeled PAH, and methotrexate had no effect. The effects of increasing stevioside and steviol concentrations on PAH and ES uptake by mouse renal cortical slices were also tested (Fig. 7A and B). Stevioside was without effect on either PAH or ES transport by the mouse renal slice at all tested concentrations (0.05 to 1 mM). On the other hand, steviol inhibited both PAH and ES uptake in a dose-dependent manner. The IC_{50} of steviol on PAH and ES uptake in renal cortical slices was 12.8 ± 3.0 and 67.6 ± 1.8 μM, respectively.

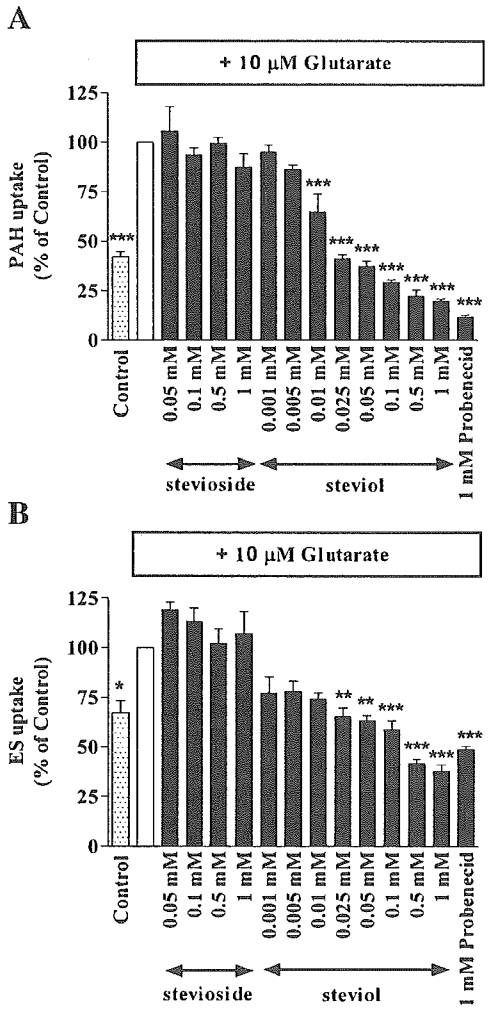

Fig. 7. The effects of stevioside and steviol on PAH (A) and ES (B) uptake in mouse renal cortical slices. Renal cortical slices were incubated in the medium containing 10 μM of [^{3}H]-PAH and 100 nM of [^{3}H]-ES with or without various concentrations of stevioside and steviol for 60 min at room temperature. The uptake was calculated as tissue/medium ratio and then transformed to a mean percentage of control. The data represent the mean ± SE of three separate experiments. Mean control T/M ratios were 5.9 ± 0.2 (PAH) and 14.3 ± 0.9 (ES), respectively. Three to five animals were used in each experiment. *$p < 0.05$, **$p < 0.01$, ***$p < 0.001$ *vs.* control.

DISCUSSION

The current study examined the interactions of stevioside and steviol with specific renal organic anion transporters using renal S2 cells expressing hOAT1, hOAT2, hOAT3, and hOAT4 and mouse renal cortical slices. The use of stable cell lines allows us to be able to determine the direct interactions of both compounds with specific human OATs. It is also desirable to confirm the predictions derived from expressed transporters with the intact renal epithelium. Because intact human renal tissues were not available, we used mouse renal cortical slices to confirm the interactions of stevioside and steviol with organic anion transporters in intact tissue.

The likely human exposure to stevioside and steviol is determined by two factors: the intake of stevioside and the extent of its metabolism to steviol. It is known that stevioside should be completely converted to steviol by intestinal microflora *in vivo* (3–5). Therefore, the "acceptable daily intake" of stevioside [7.9 mg/kg BW/day (11)] would yield a maximum plasma concentration of steviol approximately 0.2 mM. It has also been shown that peak plasma steviol concentration was 18 μM 8 h after single oral administration of *Stevia* extract (equimolar dose of 45 mg/kg BW steviol), whereas 15 min after oral administration of steviol itself (45 mg/kg BW), plasma steviol reached a peak of 57.4 μM (29). Based on these estimates, we have used concentrations of 0.05 to 1 mM for stevioside and 0.01 to 1 mM for steviol to bracket the likely exposure experienced by man.

Stevioside

Previously, it was demonstrated that stevioside at a pharmacological concentration (0.7 mM) had a small and reversible inhibitory effect on rabbit renal proximal tubular transport of PAH but had no effect on cellular ATP content and Na^+/K^+-ATPase activity (15). On the other hand, its metabolite, steviol, at very low concentration demonstrated

significant inhibition of PAH transepithelial transport. Although the precise mechanisms by which stevioside and steviol inhibited transepithelial transport of PAH were still unclear, the authors proposed that stevioside and steviol might inhibit and/or interfere with the basolateral OATs (16). However, these studies examined the net transepithelial transport of PAH at the tubular level, which may involve several OATs. Thus, the current study was performed to determine which specific organic anion transporter(s) in the renal proximal tubule interacted with stevioside and steviol. We first studied the interactions of these compounds with a single organic anion transporter expressed in renal S2 cells. These results showed that stevioside at concentrations of 50 μM to 1 mM did not inhibit organic anion uptake in S2hOAT1, S2hOAT2, S2hOAT3, and S2hOAT4 cells. Similarly, stevioside showed no inhibitory effect on PAH and ES uptake in mouse renal cortical slices (Fig. 6A, B, 7A and B). Thus, there was no evidence that stevioside altered the function of any OAT. Stevioside's lack of interaction with human OATs may be due to its large size, as it is composed of one molecule of steviol and three of glucose, and its lack of charge at physiological pH (Fig. 1), making it unlikely to access the substrate binding site on the various OATs. Although our results were clear for human and mouse OATs, Jutabha *et al.* (15) found a small reversible inhibitory effect of stevioside on PAH transport of rabbit renal proximal tubule. One possible explanation for this discrepancy may be that, at the high concentration used in the rabbit study (0.7 mM), sufficient concentrations of inhibitory stevioside derivatives may have been present to reduce transport. It is also possible that these findings may reflect species differences. Certainly, differences in substrate recognition and transport properties of organic anion transporters among species have been observed (30,31). Previous studies have also reported that renal elimination of stevioside involved its net secretion *in vivo* (32,33). However, in light of our data (above) indicating complete lack of interactions between stevioside and organic anion transporters (hOAT1, hOAT2, hOAT3, and hOAT4), one must argue that stevioside secretion does not involve organic anion transporters. Once again, there are several possible explanations for the *in vivo* findings. First, as noted above, the stevioside used in the *in vivo* studies might contain other stevioside derivatives, or it is possible that some stevioside metabolism occurred after its injection. In either instance, those derivatives or metabolites may have been excreted and detected as stevioside. Another possibility is that other transporters may play a role in the renal transport of stevioside. Recently, a novel organic anion transporting polypeptide (OATP4C1) has been cloned and shown to be expressed at the basolateral membrane of the proximal tubule (34). Because it handles organic anions including digoxin, a large cardiac glycoside, it is possible that OATP4C1 may mediate stevioside uptake and secretion. However, this possibility has not yet been explored.

To directly assess the potential of basolateral transport and accumulation of stevioside and/or steviol to induce renal tubular damage, we measured the cytotoxicity of both compounds in hOAT1- and hOAT3-expressing mouse S2 cells. As shown in Fig. 5A, 1 to 100 μM stevioside did not suppress viability in any of the cell lines S2hOAT1, S2hOAT3, and S2mock cells. In the only other study of stevioside nephrotoxicity, Toskulkao *et al.* (14,35) reported that 6.25–100 μM stevioside induced toxicity in rat renal cortical slices. However, the purity of the stevioside ≥90%, as compared to ≥98% used in our study, very likely explains the lower toxicity that we observed.

Steviol

As noted above, stevioside can be degraded to steviol by the intestinal microflora from various animal species including man (3–5). Recently, steviol has been found to inhibit transepithelial transport of PAH (J_{PAH}) by isolated perfused rabbit renal proximal tubule (16). Entirely consistent with these findings, the current study showed that steviol inhibited organic anion uptake mediated by S2 cells expressing hOAT1, hOAT2, hOAT3, and hOAT4. Both hOAT1 and hOAT3 showed high affinity for steviol (IC_{50} was 11.4 and 36.5 μM for hOAT1 and hOAT3, respectively), hOAT4 (IC_{50} = 285 μM) was intermediate, and hOAT2 exhibited the lowest affinity (IC_{50} = 1 mM). Steviol inhibition of both hOAT1 and hOAT3 was dose-dependent (Fig. 2A and B). Likewise, steviol effectively inhibited PAH and ES transport in mouse renal cortical slices (IC_{50} of steviol was 12.8 ± 3.0 and 67.6 ± 1.8 μM, respectively). Thus, steviol was a potent inhibitor of hOAT1 and hOAT3 when expressed in S2 cells as well as with mouse OAT1 and OAT3 in the intact renal epithelium. The third basolateral OAT, that is, hOAT2, showed a much lower affinity for steviol (IC_{50} = 1 mM) and is unlikely to be involved in steviol secretion.

However, hOAT4, the only apical transporter studied (20), had a modest affinity for steviol (IC_{50} = 285 μM). Thus, it may not be the primary transporter that is responsible for the exit step of steviol from cells, suggesting involvement of other apical transporters in the luminal exit of steviol. Possibilities include the human multidrug resistance-associated proteins 2 (MRP2) (36), Na^+-phosphate cotransporter (NPT1) (37), and a novel voltage-driven organic anion transporter (OAT_V1) that has recently been cloned from pig renal proximal tubules (38).

Interestingly, as shown in Figs. 2A, B, 7A, and B, steviol inhibited PAH and ES uptake in both stable cell lines and renal cortical slices as effectively as several well-known inhibitors of organic anion transport, including furosemide, bumetanide, probenecid, and indomethacin. This result raises the possibility that steviol may alter the pharmacodynamics of anionic drugs, parallelling the effects of these agents. For example, probenecid is not only a potent organic anion inhibitor, but it is also widely used in combination therapy to increase half-life of the drugs in the blood circulation. Coadministration of probenecid inhibited renal excretion of furosemide, ciprofloxacin, benzylpenicillins, and acyclovir (39–41). The current study found that the IC_{50} of steviol was similar to that of probenecid on hOAT1-mediated PAH uptake (11.4 ± 0.3 μM and 11.9 ± 1.4 μM), indicating that hOAT1 has high affinity for steviol similar to probenecid. Likewise, the affinity of hOAT3 for steviol was also substantial (IC_{50} 36.5 ± 2.6 μM) but lower than that of probenecid (IC_{50} 4.7 ± 1.0 μM). Because the basolateral entry step of organic compounds is known to be a rate-limiting step in organic anion secretion, inhibition of basolateral OAT

activity would be expected to affect the plasma level of various organic anions including therapeutic drugs and could result in either enhanced therapeutic efficacy or increased toxic side effects of the drugs. In addition, steviol at high concentrations (25–100 μM) was shown to decrease cell viability in both hOAT1- and hOAT3-expressing cell lines, whereas the control S2mock cells were much more resistant (Fig. 5B). The basis for differential toxicity would appear to be the hOAT1- or hOAT3-mediated entry of steviol into these cell lines. Because steviol has previously been shown to inhibit oxidative phosphorylation in isolated rat liver mitochondria (42), it is likely that at higher concentrations (25–100 μM), OAT-mediated entry of steviol leads to decreased energy production and increased toxicity. At lower concentration (10 μM), steviol did not show any effects on cell viability in all of cell types (Figs. 2A, B, and 5B). Thus, it is possible, due to its high potency, that low concentrations of steviol might have application as an inhibitor of OAT1 and OAT3. Conversely, steviol does pose the risk of steviol-drug interactions through competition for basolateral and apical OATs taken concurrently with stevioside or steviol.

In conclusion, data from both stable cell lines expressing human organic anion transporters and in intact renal epithelium suggest that stevioside does not interact with renal organic anion transport. In contrast, steviol directly inhibited both hOAT1 and hOAT3 with high potency. HOAT2 and hOAT4 were less effectively inhibited. Stevioside had no effect on cell viability, whereas steviol at high concentrations suppressed cell viability in renal S2 cells expressing OAT transporters. The inhibitory potency of steviol toward hOAT1 and hOAT3 was similar to that of probenecid, suggesting that steviol might have potential as an inhibitor to delay the clearance or disposal of any organic anion including therapeutic drugs mediated by renal OATs from the body. On the other hand, steviol's ability to effectively inhibit organic anion transporters raises the possibility of steviol-drug interactions through competition for elimination.

ACKNOWLEDGMENTS

We thank Dr. Chaivat Toskulkao (Department of Physiology, Faculty of Science, Mahidol University, Thailand) for kindly providing the stevioside and steviol used in this study. We are also grateful to Ramsey Walden (Laboratory of Pharmacology and Chemistry, NIEHS Research Triangle Park, NC, USA) for his assistance with renal cortical slices preparation and to Ms. Kanoknetr Suksen (Department of Physiology, Faculty of Science, Mahidol University, Thailand) for her assistance with cell viability study. This work was financially supported by the Thailand Research Fund through the Royal Golden Jubilee Ph.D. Program (grant no. PHD/0044/2544 and no. BGJ4580017).

REFERENCES

1. M. Bridel and R. Lavieille. The sweet principle of Kaa-he-e (*Stevia rebaudiana*). *J. Pharm. Clin.* **14**:99–154 (1931).
2. J. M. Geuns. Stevioside. *Phytochemistry* **64**:913–921 (2003).
3. A. M. Hutapea, C. Toskulkao, D. Buddhasukh, P. Wilairat, and T. Glinsukon. Digestion of stevioside, a natural sweetener, by various digestive enzymes. *J. Clin. Biochem. Nutr.* **23**:177–186 (1997).
4. C. Gardana, P. Simonetti, E. Canzi, R. Zanchi, and P. Pietta. Metabolism of stevioside and rebaudioside A from *Stevia rebaudiana* extracts by human microflora. *J. Agric. Food Chem.* **51**: 6618–6622 (2003).
5. E. Koyama, N. Sakai, Y. Ohori, K. Kitazawa, O. Izawa, K. Kakegawa, A. Fujino, and M. Ui. Absorption and metabolism of glycosidic sweeteners of stevia mixture and their aglycone, steviol, in rats and humans. *Food Chem. Toxicol.* **41**:875–883 (2003).
6. P. Chan, D. Y. Xu, J. C. Liu, Y. J. Chen, B. Tomlinson, W. P. Huang, and J. T. Cheng. The effect of stevioside on blood pressure and plasma catecholamines in spontaneously hypertensive rats. *Life Sci.* **63**:1679–1684 (1998).
7. P. Chan, B. Tomlinson, Y. J. Chen, J. C. Liu, M. H. Hsieh, and J. T. Cheng. A double-blind placebo-controlled study of the effectiveness and tolerability of oral stevioside in human hypertension. *Br. J. Clin. Pharmacol.* **50**:215–220 (2000).
8. Y. H. Hsu, J. C. Liu, P. F. Kao, C. N. Lee, Y. J. Chen, M. H. Hsieh, and P. Chan. Antihypertensive effect of stevioside in different strains of hypertensive rats. *Zhonghua Yi Xue Za Zhi (Taipei)* **65**:1–6 (2002).
9. J. C. Liu, P. K. Kao, P. Chan, Y. H. Hsu, C. C. Hou, G. S. Lien, M. H. Hsieh, Y. J. Chen, and J. T. Cheng. Mechanism of the antihypertensive effect of stevioside in anesthetized dogs. *Pharmacology* **67**:14–20 (2003).
10. P. B. Jeppesen, S. Gregersen, S. E. Rolfsen, M. Jepsen, M. Colombo, A. Agger, J. Xiao, M. Kruhoffer, T. Orntoft, and K. Hermansen. Antihyperglycemic and blood pressure-reducing effects of stevioside in the diabetic Goto-Kakizaki rat. *Metabolism* **52**:372–378 (2003).
11. L. Xili, B. Chengjiany, X. Eryi, S. Reiming, W. Yuengming, S. Haodong, and H. Zhiyian. Chronic oral toxicity and carcinogenicity study of stevioside in rats. *Food Chem. Toxicol.* **30**: 957–965 (1992).
12. C. Toskulkao, L. Chaturat, P. Temcharoen, and T. Glinsukon. Acute toxicity of stevioside, a natural sweetener, and its metabolite, steviol, in several animal species. *Drug Chem. Toxicol.* **20**: 31–44 (1997).
13. M. Matsui, K. Matsui, Y. Kawasaki, Y. Oda, T. Noguchi, Y. Kitagawa, M. Sawada, M. Hayashi, T. Nohmi, K. Yoshihira, J. Ishidate, and M. T. Sofuni. Evaluation of the genotoxicity of stevioside and steviol using six *in vitro* and one *in vivo* mutagenicity assays. *Mutagenesis* **11**:573–579 (1996).
14. C. Toskulkao, W. Deechakawan, P. Temcharoen, D. Buddhasukh, and T. Glinsukon. Nephrotoxic effects of stevioside and steviol in rat renal cortical slices. *J. Clin. Biochem. Nutr.* **16**:123–131 (1994).
15. P. Jutabha, C. Toskulkao, and V. Chatsudthipong. Effect of stevioside on PAH transport by isolated perfused rabbit renal proximal tubule. *Can. J. Physiol. Pharm.* **78**:737–744 (2000).
16. V. Chatsudthipong and P. Jutabha. Effect of steviol on para-aminohippurate transport by isolated perfused rabbit renal proximal tubule. *J. Pharmacol. Exp. Ther.* **298**:1120–1127 (2001).
17. M. Hosoyamada, T. Sekine, Y. Kanai, and H. Endou. Molecular cloning and functional expression of a multispecific organic anion transporter from human kidney. *Am. J. Physiol., Renal Physiol.* **276**:F122–F128 (1999).
18. S. H. Cha, T. Sekine, J. I. Fukushima, Y. Kanai, Y. Kobayashi, T. Goya, and H. Endou. Identification and characterization of human organic anion transporter 3 expressing predominantly in the kidney. *Mol. Pharmacol.* **59**:1277–1286 (2001).
19. H. Motohashi, Y. Sakurai, H. Saito, S. Masuda, Y. Urakami, M. Goto, A. Fukatsu, O. Ogawa, and K. Inui. Gene expression levels and immunolocalization of organic ion transporters in the human kidney. *J. Am. Soc. Nephrol.* **13**:866–874 (2002).
20. S. H. Cha, T. Sekine, H. Kusuhara, E. Yu, J. Y. Kim, D. K. Kim, Y. Sukiyama, Y. Kanai, and H. Endou. Molecular cloning and characterization of multispecific organic anion transporter 4 expressed in the placenta. *J. Biol. Chem.* **275**:4507–4512 (2000).
21. E. Babu, M. Takeda, S. Narikawa, Y. Kobayashi, T. Yamamoto, S. H. Cha, T. Sekine, D. Sakthisekaran, and H. Endou. Human organic anion transporters mediate the transport of tetracycline. *Jpn. J. Pharmacol.* **88**:69–76 (2002).

22. M. Takeda, S. Khamdang, S. Narikawa, H. Kimura, M. Hosoyamada, S. H. Cha, T. Sekine, and H. Endou. Characterization of methotrexate transport and its drug interactions with human organic anion transporters. *J. Pharmacol. Exp. Ther.* **302**:666–671 (2002).
23. A. Enomoto, M. Takeda, M. Shimoda, S. Narikawa, Y. Kobayashi, T. Yamamoto, T. Sekine, S. H. Cha, and T. Niwa. Interaction of human organic anion transporters 2 and 4 with organic anion transport inhibitors. *J. Pharmacol. Exp. Ther.* **301**:797–802 (2002).
24. Y. Cheng and W. H. Prusoff. Relationship between the inhibition constant (K1) and the concentration of inhibitor which causes 50 per cent inhibition (I50) of an enzymatic reaction. *Biochem. Pharmacol.* **22**:3099–3108 (1973).
25. P. Skehan, R. Storeng, D. Scudiero, A. Monks, J. McMahon, D. Vistica, J. T. Warren, H. Bokesch, S. Kenney, and M. R. Boyd. New colorimetric cytotoxicity assay for anticancer-drug screening. *J. Natl. Cancer Inst.* **82**:1107–1112 (1990).
26. J. B. Pritchard. Intracellular alpha-ketoglutarate controls the efficacy of renal organic anion transport. *J. Pharmacol. Exp. Ther.* **274**:1278–1284 (1995).
27. D. H. Sweet, L. M. Chan, R. Walden, X. P. Yang, D. S. Miller, and J. B. Pritchard. Organic anion transporter 3 (Slc22a8) is a dicarboxylate exchanger indirectly coupled to the Na^+ gradient. *Am. J. Physiol., Renal Physiol.* **284**:F763–F769 (2003).
28. J. B. Pritchard. Rat renal cortical slices demonstrate *p*-aminohippurate/glutarate exchange and sodium/glutarate coupled *p*-aminohippurate transport. *J. Pharmacol. Exp. Ther.* **255**:969–975 (1990).
29. E. Koyama, K. Kitazawa, Y. Ohori, O. Izawa, K. Kakegawa, A. Fujino, and M. Ui. *In vitro* metabolism of the glycosidic sweeteners, stevia mixture and enzymatically modified stevia in human intestinal microflora. *Food Chem. Toxicol.* **41**:359–374 (2003).
30. G. Burckhardt, A. Bahn, and N. A. Wolff. Molecular physiology of renal *p*-aminohippurate secretion. *News Physiol. Sci.* **16**:114–118 (2001).
31. S. H. Wright and W. H. Dantzler. Molecular and cellular physiology of renal organic cation and anion transport. *Physiol. Rev.* **84**:987–1049 (2003).
32. M. S. Melis. Renal excretion of stevioside in rats. *J. Nat. Prod.* **55**:688–690 (1992).
33. V. N. Cardoso, M. F. Barbosa, E. Muramoto, C. H. Mesquita, and M. A. Almeida. Pharmacokinetic studies of 131I-stevioside and its metabolites. *Nucl. Med. Biol.* **23**:97–100 (1996).
34. T. Mikkaichi, T. Suzuki, T. Onogawa, M. Tanemoto, H. Mizutamari, M. Okada, T. Chaki, S. Masuda, T. Tokui, N. Eto, M. Abe, F. Sato, M. Unno, T. Hishinuma, K. Inui, S. Ito, J. Goto, and T. Abe. Isolation and characterization of a digoxin transporter and its rat homologue expressed in the kidney. *Proc. Natl. Acad. Sci. USA* **101**:3569–3574 (2004).
35. C. Toskulkao, W. Deechakawan, V. Leardkamolkarn, T. Glinsukon, and D. Buddhasukh. The low calorie natural sweetener stevioside-nephrotoxicity and its relationship to urinary enzyme excretion in the rat. *Phytother. Res.* **8**:281–286 (1994).
36. T. P. Schaub, J. Kartenbeck, J. Konig, O. Vogel, R. Witzgall, W. Kriz, and D. Keppler. Expression of the MRP2 gene-encoded conjugate export pump in human kidney proximal tubules and in renal cell carcinoma. *J. Am. Soc. Nephrol.* **10**:1159–1169 (1999).
37. H. Uchino, I. Tamai, K. Yamashita, Y. Minemoto, Y. Sai, H. Yabuuchi, K. Miyamoto, E. Takeda, and A. Tsuji. *p*-Aminohippuric acid transport at renal apical membrane mediated by human inorganic phosphate transporter NPT1. *Biochem. Biophys. Res. Commun.* **270**:254–259 (2000).
38. P. Jutabha, Y. Kanai, and M. Hosoyamada. Identification of a novel voltage-driven organic anion transporter present at apical membrane of renal proximal tubule. *J. Biol. Chem.* **278**:27930–27938 (2003).
39. D. Overbosch, C. Van Gulpen, J. Hermans, and H. Mattie. The effect of probenecid on the renal tubular excretion of benzylpenicillin. *Br. J. Clin. Pharmacol.* **25**:51–58 (1988).
40. U. Jaehde, F. Sorgel, A. Reiter, G. Sigl, K. G. Naber, and W. Schunack. Effect of probenecid on the distribution and elimination of ciprofloxacin in humans. *Clin. Pharmacol. Ther.* **58**:532–541 (1995).
41. Y. Uwai, H. Saito, Y. Hashimoto, and K. I. Inui. Interaction and transport of thiazide diuretics, loop diuretics, and acetazolamide via rat renal organic anion transporter rOAT1. *J. Pharmacol. Exp. Ther.* **295**:261–265 (2000).
42. A. K. Bracht, M. Alvarez, and A. Bracht. Effect of *Stevia rebaudiana* natural products on rat liver mitochondria. *Biochem. Pharmacol.* **34**:873–882 (1985).

Available online at www.sciencedirect.com
SCIENCE DIRECT
ELSEVIER
Toxicology and Applied Pharmacology 210 (2006) 200 – 211
Toxicology and Applied Pharmacology
www.elsevier.com/locate/ytaap

Prenatal 3,3′,4,4′,5-pentachlorobiphenyl exposure modulates induction of rat hepatic CYP 1A1, 1B1, and AhR by 7,12-dimethylbenz[*a*]anthracene

Shin Wakui[a,*], Kiyofumi Yokoo[a], Hiroyuki Takahashi[b], Tomoko Muto[c], Yoshihiko Suzuki[d], Yoshikatsu Kanai[c], Hiroshi Hano[b], Masakuni Furusato[e], Hitoshi Endou[c]

[a]*Department of Toxicologic Pathology, Azabu University School of Veterinary Medicine, 1-17-71 Fuchinobe, Kanagawa 229-8501, Japan*
[b]*Department of Pathology, The Jikei University School of Medicine, Tokyo 105-8461, Japan*
[c]*Department of Pharmacology and Toxicology, Kyorin University School of Medicine, Tokyo 181-8611, Japan*
[d]*Department of Biochemistry, Azabu University School of Veterinary Medicine, Kanagawa 229-8501, Japan*
[e]*Department of Pathology, Kyorin University School of Medicine, Tokyo 181-8611, Japan*

Received 8 February 2005; accepted 30 April 2005
Available online 28 June 2005

Abstract

We previously reported the finding that prenatal exposure to a relatively low dose of PCB126 increases the rate of DMBA-induced rat mammary carcinoma, while a high dose decreased it. One of the most important factors determining the sensitivity to mammary carcinogenesis is the metabolic stage at administration of the carcinogenic agent. DMBA is a procarcinogen that recruits the host metabolism to yield its ultimate carcinogenic form, and CYP1A1 and CYP1B1 (CYP1) conduct this metabolism. We investigated the hepatic expression of CYP1 and AhR following oral administration of DMBA (100 mg/kg b.w.) (i.g.) to 50-day-old female Sprague–Dawley rats whose dams had been treated (i.g.) with 2.5 ng, 250 ng, 7.5 μg of PCB126/kg or the vehicle on days 13 to 19 post-conception. Real-time quantitative RT-PCR analysis revealed that the prenatal exposure to a relatively low dose of PCB126 (the 250 ng group) prolonged the higher expression of CYP1A1, CYP1B1, and AhR mRNA, while prenatal exposure to a high dose of PCB126 (the 7.5 μg group) prolonged the higher expression of CYP1A1 and AhR mRNA. Western blotting and immunohistochemical analyses were consistent with mRNAs changes. Because DMBA oxidation produces a highly mutagenic metabolite and is finally catalyzed by CYP1B1, a relatively low PCB126 dose might produce the biological character to potentially increase the risk of DMBA-induced mammary carcinoma.

Keywords: PCB126; DMBA; CYP1; AhR; Liver; Rat

Introduction

Polychlorinated biphenyls (PCBs) are a heterogeneous group of man-made organic compounds that are widely present in the environment (IARC, 1997). The chemical stability and lipophilicity of PCBs and their resistance to degradation results in their persistence and concentration in food chains (Bro-Rasmussen, 1996) as well as their bioaccumulation in human adipose tissue (Kutz et al., 1991), blood (Murphy and Harvey, 1985), and breast milk (Rogan et al., 1987). Moreover, transplacental and lactational transfers of PCBs to a developing fetus and infant have the potential to cause adverse effects (Safe and Krishnan, 1995; van den Berg et al., 1998).

7,12-Dimethylbenz[*a*]anthracene (DMBA) is a model compound that induces mammary carcinogenesis in rodents (Huggins et al., 1961; MacDonald et al., 2001; Rowlands et

Abbreviations: PCBs, polychlorinated biphenyls; CYP, cytochrome P450; AhR, aryl hydrocarbon receptor; ARNT, AhR nuclear translocator protein; PCB126, 3,3′,4,4′,5-pentachlorobiphenyl; DMBA, 7,12-dimethylbenz[*a*]anthracene.

* Corresponding author. Fax: +81 42 754 7661.
E-mail address: wakui@azabu-u.ac.jp (S. Wakui).

0041-008X/$ - see front matter © 2005 Elsevier Inc. All rights reserved.
doi:10.1016/j.taap.2005.04.022

al., 2001). We previously found that prenatal exposure to a relatively low dose of 3,3′,4,4′,5-pentachlorobiphenyl (PCB126) increases rat mammary carcinoma induced by DMBA ingestion at 50 days old, and exposure to a high dose of PCB126 acts as an inhibiting agent for it (Muto et al., 2001). One of the most important factors determining sensitivity to mammary carcinogenesis is the metabolic stage of the carcinogenic agent. DMBA is a procarcinogen and requires metabolic conversion to its ultimate carcinogenic metabolite by oxidation, which is conducted by CYP1A1 and 1B1 (CYP1) (Christou et al., 1987; Dipple, 1995; Shimada et al., 1996). Both the proximate and ultimate metabolites of DMBA that are formed in hepatocytes can be transported to other organs, resulting in carcinogen-adducted DNA (Di Giovanni and Juchau, 1980; Ginsberg and Atherholt, 1989). Therefore, the liver has a primary role in the metabolism of DMBA and is the most significantly affected organ following the experimental exposure of DMBA to an animal (Di Giovanni and Juchau, 1980; Kothari and Subramanian, 1992). Thus, the extent to which DNA adducts occur after administration of DMBA depends on the level of oxidative metabolism of DMBA due to CYP1 activities (Dipple et al., 1999; Granberg et al., 2000; MacDonald et al., 2001; Rowlands et al., 2001).

Both PCB126, a prototypical coplanar halogenated aromatic hydrocarbon, and DMBA, a polycyclic aromatic hydrocarbon, bind and activate the aryl hydrocarbon receptor (AhR), which is a basic helix–loop–helix (b-HLH) protein (Burback et al., 1992). Ligand binding results in activation of AhR and subsequent nuclear translocation, where it heterodimerizes with another bHLH partner, the AhR nuclear translocator protein (ARNT) (Hoffman et al., 1991). The AhR–ARNT dimer binds to specific regulatory elements, xenobiotic responsive elements (XREs), upstream of the responsive genes and enhances their transcripts, the CYP1 enzyme family (Dolwick et al., 1993; Jones et al., 1986; Okey et al., 1994; Rowlands et al., 2001; Schmidt and Bradfield, 1996). Enzyme activation of carcinogens yields intermediate metabolites that are chemically more reactive than the initial compound (Cavalieri et al., 2002). Hence, we investigated the expressions of hepatic CYP1 and AhR following ingestion of DMBA by 50-day-old offspring of female rats that had been exposed to PCB126 on days 13 to 19 post-conception.

Materials and methods

Animals, chemicals, and treatments. Forty-five female and nine male 6-week-old Sprague–Dawley (slc) rats (Japan SLC, Shizuoka, Japan) were housed, three per plastic cage, on hardwood-chip bedding in an environment-controlled room on a 12-h light/12-h dark cycle at 22 ± 2 °C and 55% ± 5% relative humidity, with a conventional diet (MF, Oriental Yeast, Tokyo, Japan). All experimental procedures were conducted following approval of the Animal Care and Use Committee of the Azabu University School of Veterinary Medicine. Guidelines set by the National Institute of Health and Public Health Service Policy on the Humane Use and Care of Laboratory Animals were followed at all times. PCB126 was obtained from AccuStandard Inc., New Haven, CT, and DMBA was obtained from Tokyo Chemical Industry Co. Ltd., Tokyo, Japan. Seven-week-old rats were housed with five females and a male per plastic cage.

A lifetime tolerable daily intake (TDI) of PCB126 has been reported to range from 10 to 100 pg/kg/day (van den Berg et al., 1998). In this study, three doses of PCB126 were selected using 25 pg/kg/day as the TDI dose (Muto et al., 2001): 10^2-fold of the TDI dose, 10^4-fold of the TDI dose, and 3×10^5-fold of the TDI dose. Groups of eight pregnant rats were treated with 2.5 ng, 250 ng, or 7.5 μg/kg body (i.g.) PCB126 or with an equivalent volume of corn oil (~0.5 ml/animal, i.g.), on days 13 through 19 post-conception. The offspring were sexed at birth, and litters were reduced so that each dam was left with eight offspring (four females/dam). Weaning was carried out at day 21 post-partum. In this study, we considered the group of rats with prenatal exposure to 2.5 ng, 250 ng, or 7.5 μg/kg body PCB126 or with an equivalent volume of corn oil as the 2.5-ng, the 250-ng, the 7.5-μg, or the vehicle group, respectively.

Each PCB126-treated group (2.5-ng, 250-ng, or 7.5-μg group) included forty-five females, and the vehicle group included thirty-six females. For experiments, 135 fifty-day-old female rats received 100 mg/kg DMBA in corn oil/kg body (i.g.), and 36 received an equivalent volume of corn oil (~0.5 ml/animal, i.g.). In this study, the dose of DMBA was selected following the study of Huggins et al. (1961) with the conversion using animal body weight. Following anesthesia by diethyl ether, liver samples were obtained under deep anesthesia from five (DMBA-fed) and four (corn oil-fed) rats from each group at 6 h, 12 h, 1 day, 2 days, 5 days, 10 days, 20 days, and 30 days. Representative sections of each liver were fixed in 10% phosphate-buffered formalin and routinely processed for immunohistochemistry. In addition, representative sections were frozen without fixation and stored at −80 °C.

Chemical analysis. Analysis for PCB126 was carried out following the alkaline alcohol digestion method (Tanabe et al., 1987). Aliquots of homogenized rat mammary tumor samples were refluxed in 1 N KOH–ethanol solution for 1 h. The PCB126 thus extracted into ethanol was transferred to 100 ml of hexane by shaking in a separating funnel. Subsequently, the hexane layer was concentrated and purified by passing it through 1.5 g of silica gel (Wako gel S-1, Wako Co., Ltd., Osaka, Japan) packed in a glass column (10 mm inside diameter × 200 mm length). PCB126 was eluted with 200 ml of hexane at an elution rate of one drop per second. The eluate was concentrated to 5 ml in a Kuderna–Danish concentrator and further purified with 5% fuming sulphuric acid. All samples were injected into a gas chromatograph-mass spectrometer (GC-MS: Shimadzu 9020

DF with an SCAP-1123 data system, Shimadzu Co. Ltd., Kyoto, Japan) equipped with an electron-impact ion-source and moving needle-type injection system for the determination and identification of PCB126. The column consisted of a 0.23 mm I.D. × 30 m glass capillary, coated with silicone. Operating conditions of the GC-MS were as follows: column oven temperature was programmed to rise from 190 °C to 250 °C at 0.5 °C min^{-1}; injector and ion-source temperatures were kept at 250 °C and 280 °C, respectively. PCB126 was determined by selected ion monitoring at *m/z* 326. The carrier flow of helium was controlled at 0.6 ml min^{-1}.

Immunohistochemistry. Immunohistochemical expressions of CYP1A1 and CYP1B1 were analyzed using the avidin–biotin complex (ABC) method. After deparaffinization, 4 μm thick sections were treated sequentially with 0.3% H_2O_2 for 10 min, then blocked with 10% goat serum or horse serum in PBS for 20 min. Sections were thawed, rinsed in PBS, and treated with primary antibodies of rabbit anti-rat-CYP1A1 (Affiniti Res. Inc., Exeter, UK; diluted 1:1000) and rabbit anti-CYP1B1 (BD Biosciences, Bedford, MA; diluted 1:50). Bound IgG was detected with biotinylated goat anti-rabbit IgG (Vector Lab., Burlingame, CA; diluted 1:100) followed by avidin–biotin complex (ABC)-peroxidase (Vector Lab., Burlingame, CA) and diaminobenzidine (Sigma, St. Louis, MO). Sections were then counterstained with hematoxylin. As a negative control, non-immunized rabbit serum was substituted for the primary antibody.

Real-time quantitative RT-PCR. For each RNA sample, 100 ng was used as the template for first strand cDNA synthesis using a TaqMan Reverse Transcription kit, following the RT-PCR manufacturer's two-step protocol (PE Applied Biosystems, Foster City, CA). Controls included for each reaction were the RNA sample without reverse transcriptase (RNA − RT) and no RNA with reverse transcriptase (no RNA + RT). The conditions of the final reaction for reverse-transcription were as follows: 1 × TaqMan RT buffer; 5.5 mM $MgCl_2$; 500 μM dATP, dGTP, and dCTP; 1 mM dTTP; Random Hexamers 0.25 μM; 1.25 Ul MuLV reverse transcriptase and 0.4 U RNase inhibitor (PE Applied Biosystems, Foster City, CA). Quantitative analyses of target gene (CYP1A1, CYP1B1, and AhR) mRNA expression were performed by real-time quantitative PCR using the ABI Prism 7700 Sequence Detection System (PE Biosystems, Foster City, CA) with Taq Man chemistry and probe. The TaqMan probes and primers for target genes were assay-on-demand gene expression products (PE Applied Biosystems, Foster City, CA) and oligonucleotides with fluorescent reporter and quencher dyes attached (Table 1). Optimal primer, probe, and cDNA concentrations were determined in a separate set of experiments to insure that both target gene and GAPDH fragments were amplified with equal efficiency. PCR reactions were performed with first-strand cDNA synthesis (2 μl) from each sample, a Universal PCR Master Mix kit (PE Applied Biosystems, Foster City, CA), 250 nM TaqMan probe, 0.16 U of AmpErase UNG (uracil N-glycosylase), and 900 nM forward-reverse primers of the target gene and GAPDH. Three measurements per sample were performed in each of two independent experiments. Results were analyzed with the ABI Sequence Detector software version 1.7 (PE Applied Biosystems, Foster City, CA). For relative quantification of target gene expression, the standard curve method was applied. The calibrated standard curve of each target gene cDNA and GAPDH amplification plots were examined at five different dilutions (containing 100, 50, 25, 10, or 5 ng) of total RNA samples that were obtained from each PCR product using a TOPO II TA Cloning Kit (Invitrogen, Carlsbad, CA) following the manufacturer's recommendations. The target gene's normalized value was determined by dividing the average target gene value by the average GAPDH value. The standard deviation (SD) of the quotient is calculated from the SD of the target gene and GAPDH using the following formula:

$$CV = (\text{SD of the quotient})/(\text{mean value of the quotient})$$

$$(CV)^2 = (CV_1)^2 + (CV_2)^2$$

$$CV_1 = (\text{SD of target gene value})/(\text{mean of target gene value})$$

$$CV_2 = (\text{SD of GAPDH value})/(\text{mean of GAPDH value})$$

The normalized target gene value is a unitless number that can be used to compare the relative amount of the target gene in different samples. One way to make this comparison is to designate one of the samples as a calibrator. In this study, the liver of 50-day-old rat of the vehicle group without DMBA ingestion was designated as the calibrator, and the averaged target gene value was divided by the average calibrator value according to the manufacturer's instructions for quantification of relative gene expression (User Bulletin #2; P/N 4303859, pp. 3–30, 36).

Western blot analysis. Rat livers were homogenized in 50 mM Tris–HCl, 150 mM KCl (pH 7.4), 1% Triton X-100, and 0.25 mM phenylmethylsulfonyl fluoride (PMSF) and centrifuged at 8000 × *g* for 30 min at 4 °C. The supernatant obtained was centrifuged at 100,000 × *g* for 90 min at 4 °C.

Table 1
ID numbers of TaqMan probes and primers (Assay-on-Demand gene expression products) used for real-time quantitative RT-PCR

Gene	ID
CYP1A1	Rn0048721_ml
CYP1B1	Rn00564055_ml
AhR	Rn00565750_ml

Assay-on-Demand gene expression products were supplied by PE Applied Biosystems, Foster City, CA.

Table 2
Body and liver weights of 50-day-old female rats after prenatal PCB126 exposure

Group	Body weight (mg)	Liver weight (mg)
7.5 μg	242.25 ± 4.07	12.06 ± 0.89
250 ng	245.32 ± 4.21	12.22 ± 0.53
2.5 ng	243.26 ± 5.82	11.70 ± 0.55
Vehicle	243.22 ± 6.22	11.86 ± 0.76

Values represent mean ± SEM Scheffé's F test, NS.

The pellet was suspended in 50 mM Tris–HCl (pH 7.4), 1% Triton X-100, and 1 mM PMSF, and the protein concentrations were determined with a bicinchonic acid protein assay reagent kit (Pierce, Rockford, IL) with bovine serum albumin as a standard. Microsomal samples were subjected to electrophoresis on a 10% SDS polyacrylamide gel using 10 μg of microsomes. The proteins were transferred for 2 h to a nitrocellulose membrane that was blocked by immersing it in 5% non-fat dried milk in phosphate-buffered saline with 0.1% (v/v) Tween 20 (PBS-T). Western blot analysis was performed using anti-rat-CYP1A1 (Affiniti Res., Exeter, UK), anti-rat-CYP1B1 (BD Gentest, San Jose, CA), or anti-AhR (H-211) (Santa Cruz, Santa Cruz, CA) antibodies. CYP1A1, CYP1B1, and AhR antibodies were diluted 1:1000, 1:500, and 1:1000, respectively, in PBS-T and incubated 1 h at room temperature on an orbital shaker. After being washed three times with PBS-T, they were incubated with a 1:2500 dilution of horseradish peroxidase-conjugated anti-rabbit antibody (Amersham Biosciences, Piscataway, NJ) for 1 h on an orbital shaker. After being washed three times with PBS-T, the membranes were detected using the ECL Plus Western Blotting Detection System (Amersham Biosciences, Piscataway, NJ).

Statistical analysis. For each set, the mean value, standard deviation, and standard error of the mean were calculated and compared using Scheffé's F test or a chi-square test using the computer statistical analysis system Stat View-J 5.0 (Abacus Concepts, Cary, NC).

Results

Body and liver weights, and concentration of PCB126 in liver

Prenatal PCB126 treatment of dams resulted in offspring with body weights and liver weights that were similar between groups at 50 days old (Table 2). The concentration of PCB126 in the liver of 50-day-old rats compared to the vehicle group was about 365 times higher in the 7.5-μg group, about 12 times higher in the 250 ng group, and about 1.5 times higher in the 2.5 ng group, and that of 80-day-old rats compared to the vehicle group was about 26 times higher in the 7.5-μg group, about 1.4 times higher in the 250-ng group, and about 1.1 times higher in the 2.5-ng group (Table 3).

Table 3
Concentration of PCB126 in livers of female rats after prenatal exposure

Group	50-day-old	80-day-old
7.5 μg	73.05 ± 8.68*	5.01 ± 3.79
250 ng	2.35 ± 1.39	0.26 ± 0.96
2.5 ng	0.30 ± 0.98	0.21 ± 0.88
Vehicle	0.20 ± 0.42	0.19 ± 0.37

Values represent mean ± SEM ng/g.
* Scheffé's F test, $P < 0.05$.

Quantitative RT-PCR for CYP1A1 and CYP1B1 mRNA expression in prenatally PCB126-exposed rat liver

In 50-day-old rats, the 7.5-μg group showed significantly increased expression of hepatic CYP1A1 mRNA (33-fold) and CYP1B1 mRNA (15-fold), and the other groups showed lower expression of CYP1A1 mRNA (1- to 3-fold) and CYP1B1 mRNA (1- to 1.7-fold) (Figs. 1, 2). As they grew older, the CYP1 mRNA expression levels of the 7.5-μg group gradually decreased, but remained at significantly higher levels compared with that of the other groups until they were 70 days old (Figs. 1, 2).

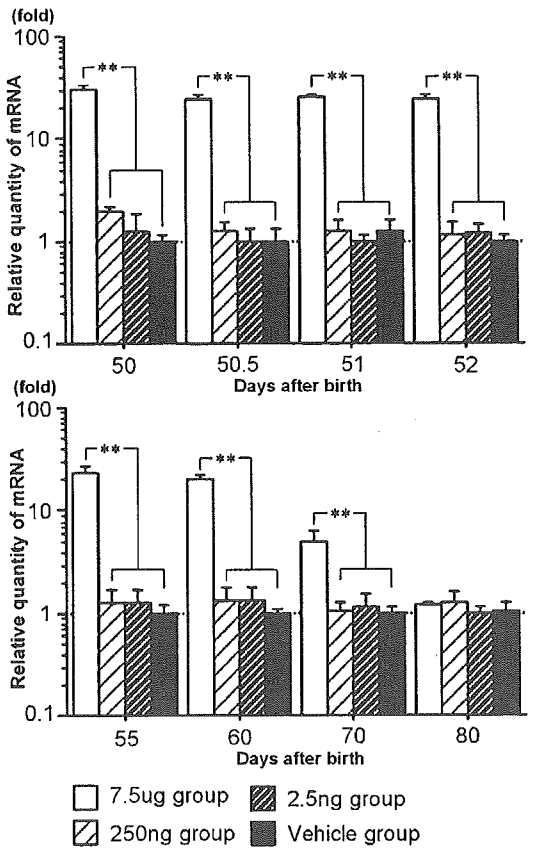

Fig. 1. Effect of prenatal exposure to PCB126 on CYP1A1 mRNA expression in rat liver. The indicated mRNA levels were determined by real-time quantitative RT-PCR, with analysis using the standard curve method described under Materials and methods. Each level was normalized to that of the endogenous housekeeping gene GAPDH in each tissue, as described under Materials and methods. Values represent mean ± SD. (**) Scheffé's F test $P < 0.01$.

Quantitative RT-PCR for CYP1A1mRNA expression following DMBA ingestion in prenatally PCB126-exposed rat liver

At 6 h after DMBA ingestion, the expression of CYP1A1 mRNA was significantly higher in all PCB126-treated groups (33- to 34-fold) than in the vehicle group (25-fold) (Fig. 3). After 12 h, all groups showed a similarly high level (Fig. 3). After 1 day, CYP1A1 mRNA expression of all PCB126-treated groups remained at high levels, but that of the vehicle group decreased to 25-fold (Fig. 3). After 2 days, CYP1A1 mRNA expression of the 7.5-μg and 250-ng groups remained at similarly high levels, but that of the 2.5 ng and vehicle groups decreased to 15- to 17-fold (Fig. 3). At 5 days after, CYP1A1 mRNA expression of the 7.5-μg and 250-ng groups showed a 28- to 32-fold increase, and that of 2.5-ng group had decreased 12-fold, while in the vehicle group, it had decreased to the calibrator level (Fig. 3). Subsequently, CYP1A1 mRNA expression of the 7.5-μg and 250-ng groups was gradually decreased to 22- to 28-fold at 10 days after, 18- to 20-fold at 20 days after, and CYP1A1 mRNA expression of the 2.5 ng and vehicle groups had returned to the calibrator level at 10 to 20 days after (Fig. 3). At 30 days after, CYP1A1 mRNA expression of all groups had returned to the calibrator level (Fig. 3).

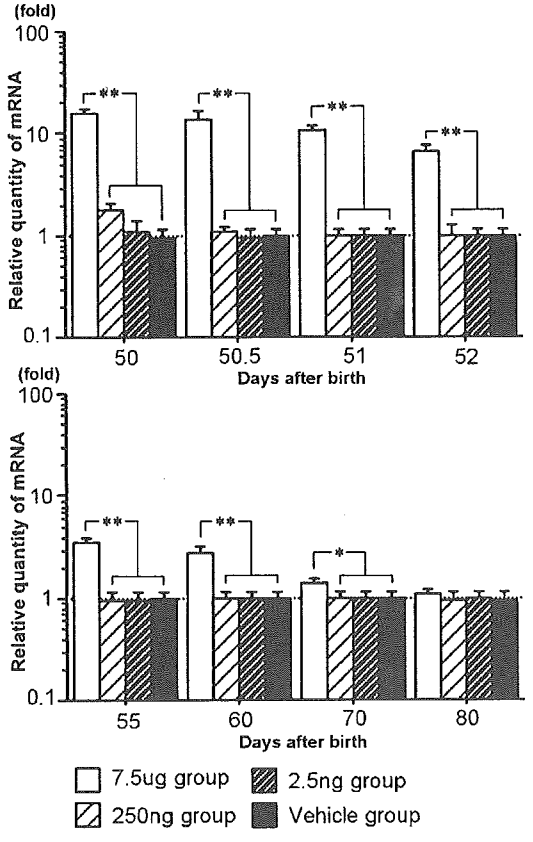

Fig. 2. Effect of prenatal exposure to PCB126 on CYP1B1 mRNA expression in rat liver. The indicated mRNA levels were determined by real-time quantitative RT-PCR, with analysis using the standard curve method described under Materials and methods. Each level was normalized to that of the endogenous housekeeping gene GAPDH in each tissue, as described under Materials and methods. Values represent mean ± SD. (**) Scheffé's F test $P < 0.01$. (*) Scheffé's F test $P < 0.05$.

Quantitative RT-PCR for CYP1B1mRNA expression following DMBA ingestion in prenatally PCB126-exposed rat liver

At 6 h after DMBA ingestion, the expression of CYP1B1 mRNA of all PCB126-treated groups had increased (24- to 26-fold), but that of the vehicle group remained at the calibrator level (Fig. 4). After 12 h to 1 day, CYP1B1 mRNA expression of the 7.5-μg and 250-ng groups increased further to 25- to 27-fold, and that of vehicle group also increased to 17- to 18-fold (Fig. 4). At 2 days after, CYP1B1 mRNA expression of the 7.5-μg and 250-ng groups remained at similarly high levels, but in the vehicle group it had decreased to 14-fold (Fig. 4). At 5 days after, CYP1B1 mRNA expression of the 250-ng group showed a 20-fold increase, which was significantly higher than that of the 7.5-μg and 2.5-ng groups (9- to 10-fold), and the vehicle group had decreased to the calibrator level (Fig. 4). After 10 to 20 days, CYP1B1 mRNA expression of the 250-ng group was 18-fold, which was significantly higher than that of the 7.5-μg group (8-fold), and the 2.5-ng and vehicle groups had returned to the calibrator level (Fig. 4). After 30 days, CYP1B1 mRNA expression of the 250-ng group was 2-fold, which was significantly higher than that of the 2.5-ng and vehicle groups (Fig. 4).

Quantitative RT-PCR for AhR mRNA expression following DMBA ingestion in prenatally PCB126-exposed rat liver

At 6 h after DMBA ingestion, the expression of AhR mRNA had increased, but those of all PCB126-treated groups (33-fold) were significantly higher than that of the vehicle group (25-fold) (Fig. 5). At 12 h after, AhR mRNA expression of all groups showed similarly high levels (Fig. 5). At 1–2 days after, AhR mRNA expression of the vehicle group gradually decreased (Fig. 5). At 5 days after, AhR mRNA expression of the 250-ng group was 35-fold, which was significantly higher than that of the 7.5-μg and 2.5-ng groups, and in the vehicle group, it had decreased to the calibrator level (Fig. 5). At 10–20 days after, AhR mRNA expression of the 250-ng group gradually decreased, but it was significantly higher than that of the 7.5-μg group, and in the 2.5-ng and vehicle groups, it was at the calibrator level (Fig. 5). After 30 days, all groups were at the calibrator level (Fig. 5).

Immunohistochemistry for CYP1A1 and CYP1B1, and Western blot analyses of CYP1A1, CYP1B1, and AhR expression following DMBA ingestion in prenatally PCB126-exposed rat liver

To determine whether the mRNA modulation of the CYP1 and AhR correlates with changes in protein expres-

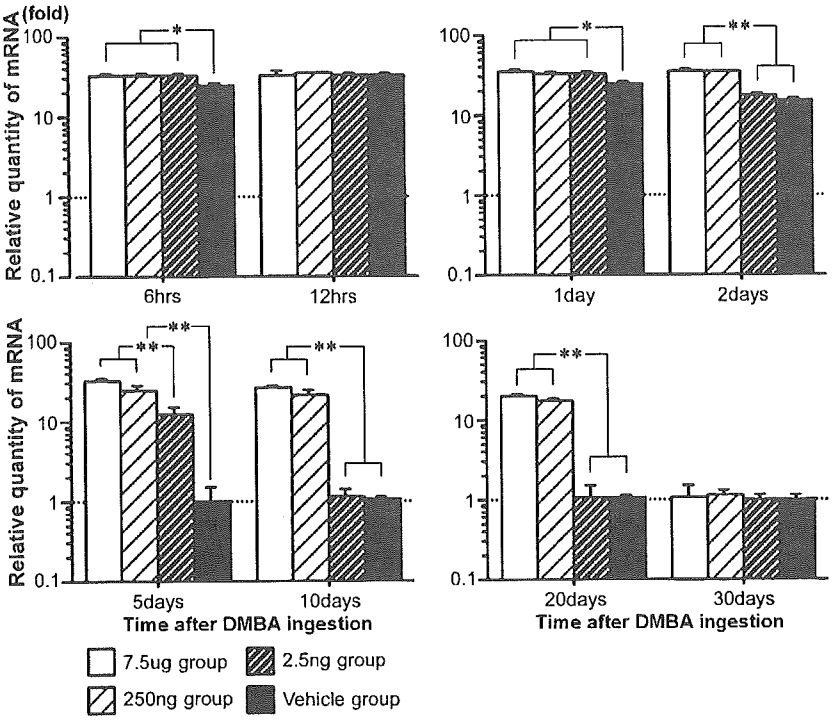

Fig. 3. Effect of prenatal exposure to PCB126 on CYP1A1 mRNA expression in rat liver following DMBA ingestion. The indicated mRNA levels were determined by real-time quantitative RT-PCR, with analysis using the standard curve method described under Materials and methods. Each level was normalized to that of the endogenous housekeeping gene GAPDH in each tissue, as described under Materials and methods. Values represent mean ± SD. (**) Scheffé's F test $P < 0.01$ (*) Scheffé's F test $P < 0.05$.

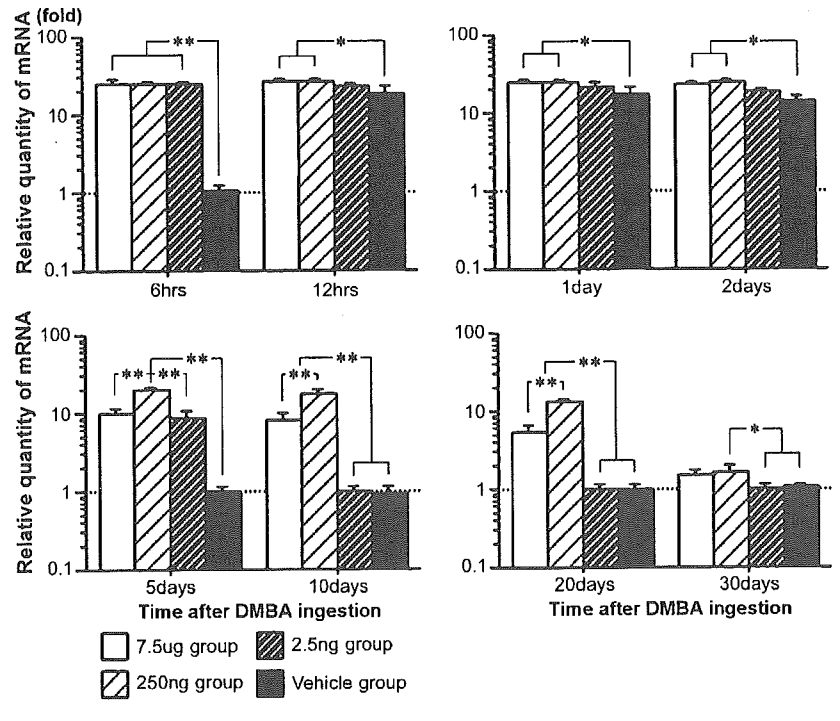

Fig. 4. Effect of prenatal exposure to PCB126 on CYP1B1 mRNA expression in rat liver following DMBA ingestion. The indicated mRNA levels were determined by real-time quantitative RT-PCR, with analysis using the standard curve method described under Materials and methods. Each level was normalized to that of the endogenous housekeeping gene GAPDH in each tissue, as described under Materials and methods. Values represent mean ± SD. (**) Scheffé's F test $P < 0.01$ (*) Scheffé's F test $P < 0.05$.

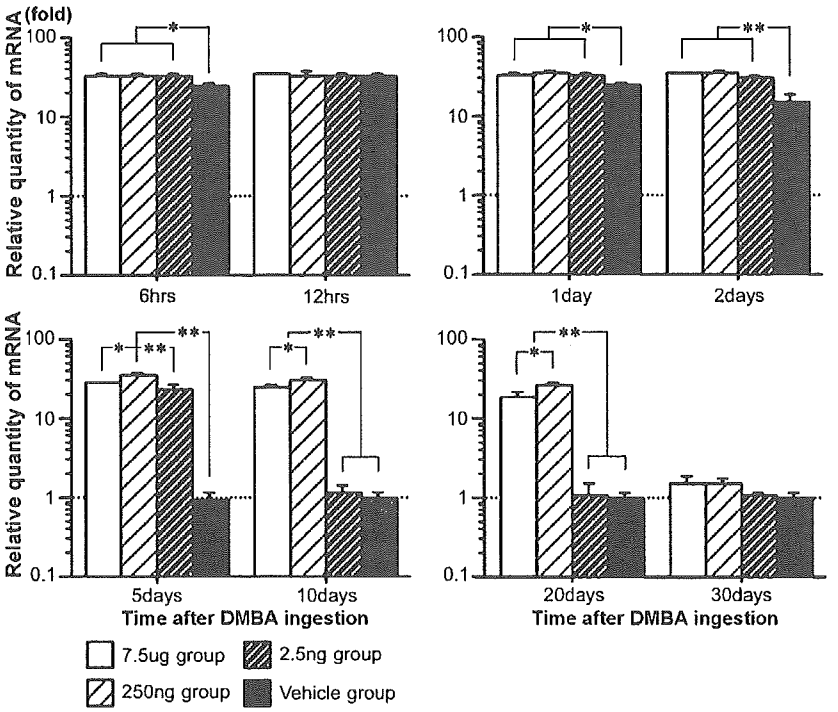

Fig. 5. Effect of prenatal exposure to PCB126 on AhR mRNA expression in rat liver following DMBA ingestion. The indicated mRNA levels were determined by real-time quantitative RT-PCR, with analysis using the standard curve method described under Materials and methods. Each level was normalized to that of the endogenous housekeeping gene control GAPDH in each tissue, as described under Materials and methods. Values represent mean ± SD. (**) Scheffé's F test $P < 0.01$ (*) Scheffé's F test $P < 0.05$.

sion, immunohistochemistry, and/or Western blot analyses were performed. The protein expression was qualitatively consistent with the patterns observed for CYP1A1 mRNA, CYP1B1 mRNA, and AhR mRNA (Figs. 6–8).

Discussion

PCBs are ubiquitous environmental contaminants that produce a spectrum of adverse biochemical and biological effects, including carcinogenic effects in people and a wide variety of animals (IARC, 1997). The induction of CYP1 expression by PCBs and DMBA has been extensively investigated (Angus et al., 1999; Christou et al., 1987; Rowlands et al., 2001; Schmidt and Bradfield, 1996; Whitlock, 1999), and it has been established that the nuclear AhR/ARNT heterodimeric complex acts as a ligand-activated transcription factor that binds to XREs in the regulatory region of CYP1 genes (Evans, 1988).

Our previous study found that rats given 250 ng PCB126/kg/day (from days 13 through 19 post-conception) had a higher incidence of DMBA-induced mammary carcinogenesis than a group given 7.5 μg PCB*126*/kg/day (from days 13 through 19 post-conception) (Muto et al., 2001). PCBs are considered non-genotoxic carcinogens because they do not produce DNA adducts and are negative for genotoxic tests (Turteltaub et al., 1990), while DMBA, a member of the polycyclic aromatic hydrocarbons (PAHs), is a procarcinogen and requires metabolic conversion to its ultimate carcinogen metabolite, DMBA-3,4-dihydrodiol-1,2-epoxide (Dipple et al., 1984; Slaga et al., 1979; Slims and Grover, 1981), by a process that includes two separate oxidations, produces 3,4-dihydrodiol, and is catalyzed by either CYP1A1 or CYP1B1 (Christou et al., 1987; Ciolino et al., 2002). The second oxidation produces the highly mutagenic 3,4-dihydrodiol-1,2-epoxide metabolite and is catalyzed by CYP1B1 (Shimada et al., 1996). These data suggest that CYP1B1 is an essential enzyme for metabolic activation, and thus the carcinogenic potential of DMBA is dependent on it. In this study, the 7.5-μg group showed higher expression of CYP1A1 until 20 days after DMBA ingestion, while the 250-ng group showed higher expression of CYP1A1 until 20 days after and higher expression of CYP1B1 until 30 days after. The mechanisms controlling the tissue-specific transcription of CYP1B1 are now not known (Sasaki et al., 2003). Our results are the first demonstration, to our knowledge, of a modulation of CYP1B1 expression by PAHs. Indeed, it has been suggested that CYP1B1 possesses a greater capacity than CYP1A1 to bioactivate a number of PAH procarcinogens (MacDonald et al., 2001; Shimada et al., 1996). Because Western blotting and immunohistochemical analyses were qualitatively consistent with each mRNA change, increased activities of these enzymes would also be revealed in the increased protein expression.

When DMBA was ingested at 50 days old, only the 7.5-μg group showed a high level of hepatic CYP1 expression, and it had decreased to that of the calibrator level at 80 days

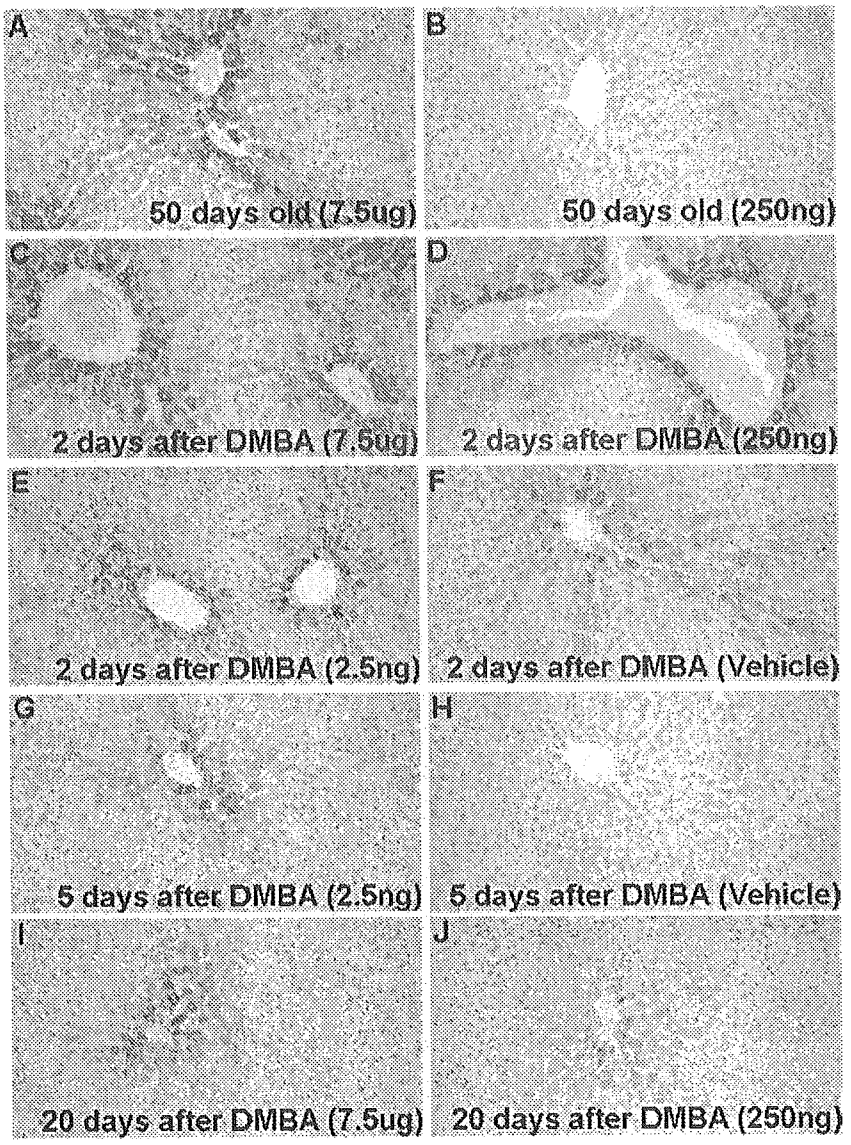

Fig. 6. Immunohistochemical analysis of CYP1A1 in rat liver. Just before DMBA ingestion, a large number of hepatocytes in the 7.5-μg group were positive (A) for CYP1A1, but negative in the 250-ng group (B). At 2 days after DMBA administration, a large number of hepatocytes were positive in the 7.5-μg (C) and 250-ng groups (D), and many hepatocytes were positive in the 2.5 ng (E) and vehicle groups (F). At 5 days after administration, some hepatocytes were positive in the 2.5-ng group (G), but none was positive in the vehicle group (H). At 20 days after DMBA administration, some hepatocytes were positive in the 7.5-μg group (I), and a few hepatocytes were positive in the 250-ng group (J). ABC method, Mayer's hematoxylin counterstain. Magnification ×140.

old. Because the 7.5-μg group possessed a high level of hepatic PCB126 residues (more than 31 times that of the other groups) on the day of DMBA ingestion, these CYP1 inductions were thought to be due to a complex induction by PCB126 residues and ingested DMBA, while the 250-ng and 2.5-ng group revealed prolonged CYP1 inductions compared to that of the vehicle group. Because the 250-ng and 2.5-ng groups showed a lower level of CYP1 with lower PCB126 residues at the time of DMBA ingestion (50 days old), it seems that prenatal exposure to PCB126 increases hepatocyte sensitivity in the rat for CYP1 induction by ingested DMBA.

The precise mechanism of the modulation of DMBA-induced mammary carcinogenesis by PCB126 remains to be explained, but one possible mechanism could be the ability of CYP1A1 and CYP1B1 to metabolize highly oxidative DMBA because carcinogenesis was dominant in the 250-ng group, while the concentration of PCB126 residues due to prenatal exposure that induced a high level of CYP1A1 was highest in the 7.5-μg group. The predominance of CYP1B1 in several human cancers, including breast carcinomas (Eltom et al., 1998; Merchant et al., 1993; Murray et al., 1997), has been reported. The functional involvement of CYP1B1 in PAH metabolism has been demonstrated by the fact that the metabolism of DMBA by microsomes from MCF-7 cells is inhibited by anti-CYP1B1 antibody, but not anti-CYP1A1 antibody (Christou et al., 1995). Although it is well known that PCBs specifically induce CYP1 (Angus et al., 1999; Christou et al., 1987; Tritscher et al., 1992), it remains to

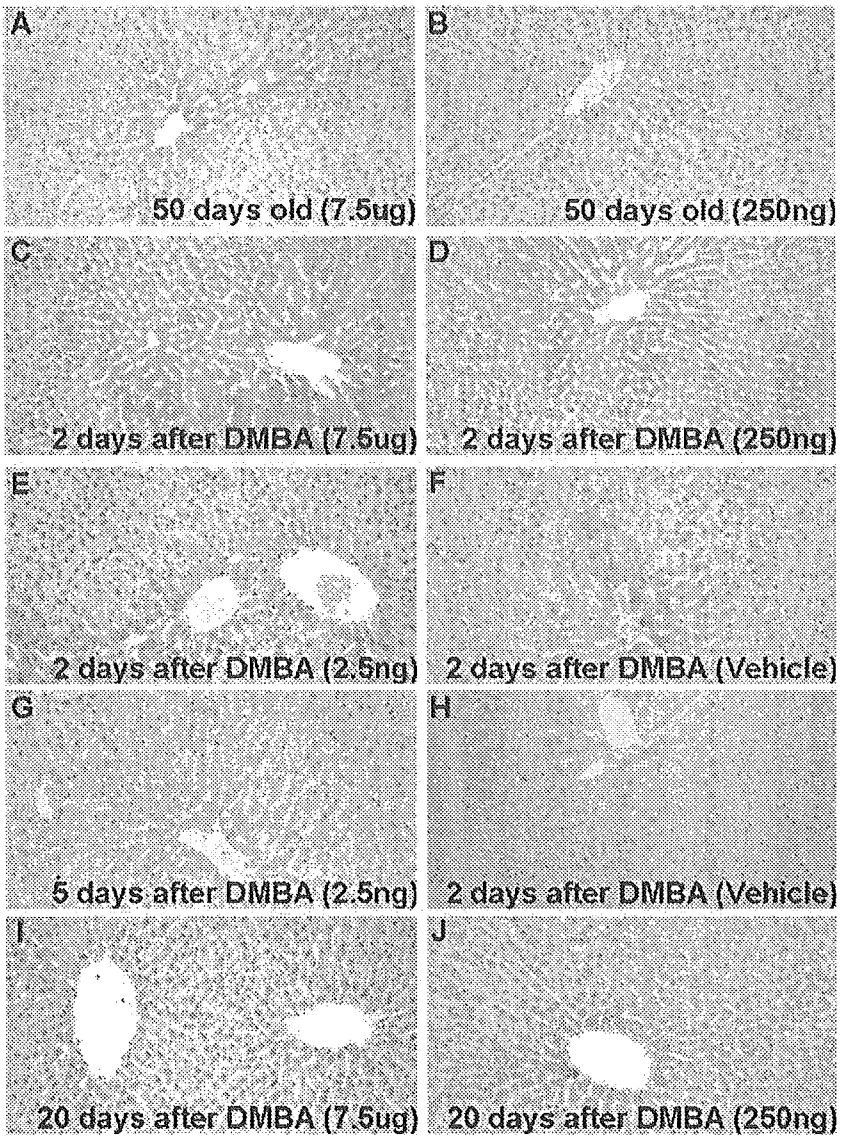

Fig. 7. Immunohistochemical analysis of CYP1B1 in rat liver. Just before DMBA ingestion, some hepatocytes in the 7.5-μg group were positive for CYP1B1 (A) but negative in the 250-ng group (B). At 2 days after DMBA administration, a large number of hepatocytes were positive in the 7.5-μg (C) and 250-ng groups (D), and many hepatocytes were positive in the 2.5 ng (E) and vehicle group (F). At 5 days after DMBA administration, some hepatocytes were positive in the 2.5 ng group (G), but none was positive in the vehicle group (H). At 20 days after DMBA administration, a few hepatocytes were positive in the 7.5-μg group (I), and some hepatocytes were positive in the 250-ng group (J). ABC method, Mayer's hematoxylin counterstain. Magnification ×140.

be determined why the 250-ng group showed higher CYP1B1 expression than the 7.5-μg group.

After DMBA was ingested to rats, previous studies have described the maximum urinary excretions of DMBA take place during the period ranging from 6 h to 1 day (Semin et al., 1976), and high levels of metabolite DMBA-DNA adducts in liver are found on days 1 to 2 (El-Bayoumy et al., 1992). Then, the large amounts of DMBA-DNA adducts in liver and mammary glands were remained to be observed at 12 days after DMBA ingestion (Daniel and Joyce, 1984), but their levels after that was unclear. Meanwhile, several previous studies have described the induction of rat hepatic CYP1 mRNA and/or protein within 1 day of DMBA ingestion (Badawi et al., 2000; Bolognesi et al., 1991; Granberg et al., 2000; Heidel et al., 1998; Moon et al., 1988; Rowlands et al., 2001). In our previous study, following DMBA ingestion without PCB126 exposure, the induction of hepatic CYP1A1 was first observed at 12 h, was revealed to peak on day 2 and decreased on day 5, and the induction of hepatic CYP1B1 was first observed on day 2 and decreased on day 5 (Muto et al., 2003). While present study revealed that prenatal PCB126 exposure rats were induced the prolongation of hepatic CYP1 induction following DMBA ingestion, especially the longer persistence of CYP1B1 induction was apparently in the 250-ng group. The implication of estradiol (E2) in breast tumorigenesis is widely documented (Nandi et al., 1995; Weinberg, 1996). An alternative mechanism of E2 carcinogenicity stems from the metabolism of this hormone, which generates several catechol derivatives from monohydroxylation reactions,

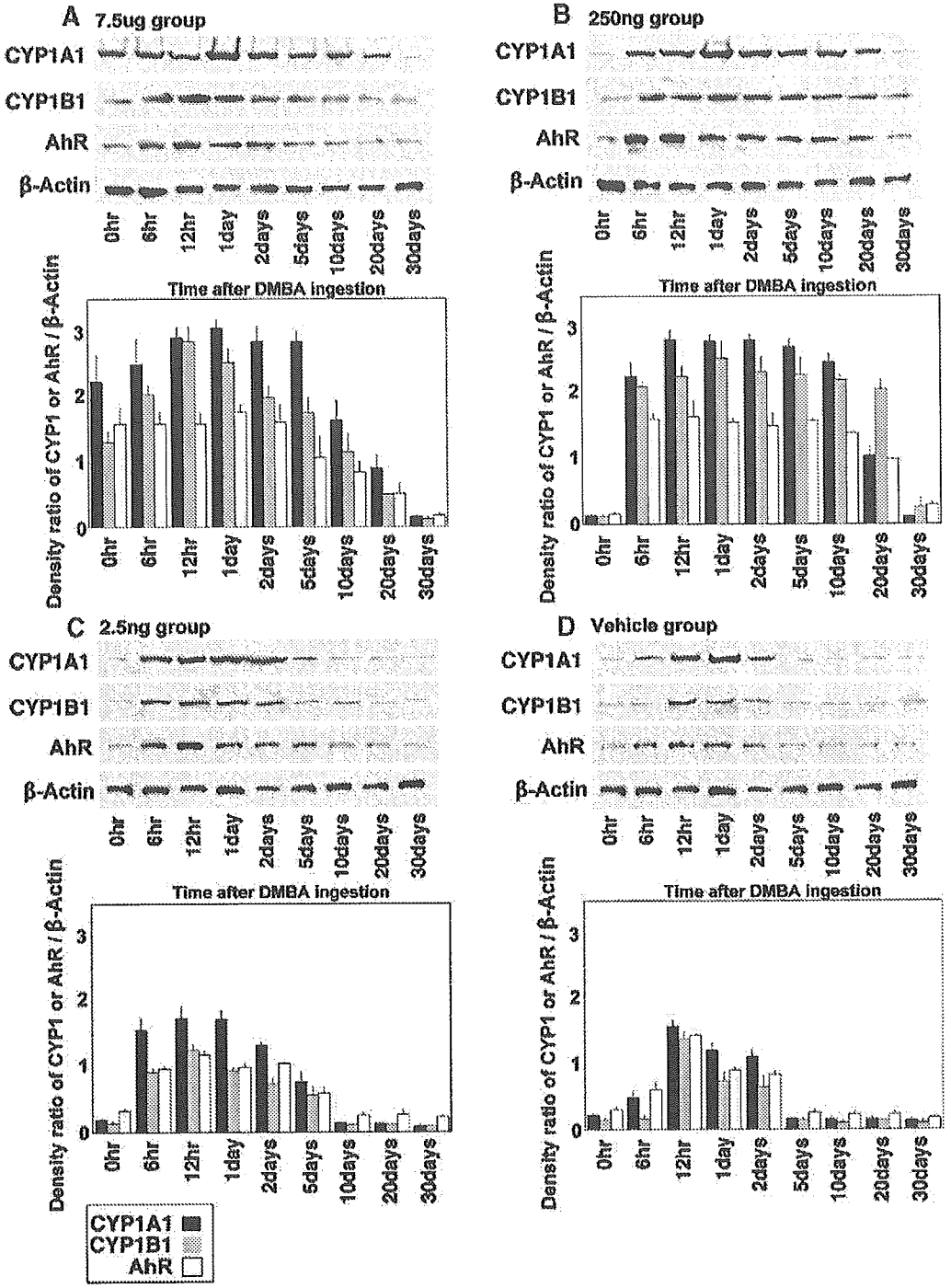

Fig. 8. Western blots of CYP1A1, CYP1B1, and AhR of rat liver following DMBA ingestion after prenatal exposure to PCB126. The protein concentration was determined with a bicinchonic acid protein assay reagent kit (Pierce) with bovine serum albumin as a standard. Ten μg of microsome samples were applied for Western blotting analysis, and immunoreactive proteins were detected using the ECL Plus Western Blotting Detection system (Amersham Biosciences, Buckinghamshire, UK). The upper panels show the representative Western blots bands of CYP1, AhR and β-actin, and the lower panels show the density ratio of CYP1, or AhR/β-actin; results are obtained by screening sample from five rats of each group. Values represent mean ± SD (A) the 7.5 μg group; (B) the 250 ng group; (C) the 2.5 ng group; (D) the vehicle group.

and liver is the primary site of E2 metabolism (Beleh et al., 1995; Waalkes et al., 2004; Wang and Liehr, 1994). This is in particular, the case of 4-hydroxylated E2, which is generated mainly by CYP1B1, displays a strong genotoxicity (Cavalieri et al., 2002; Safe and Krishnan, 1995). On the other hand, CYP1A1 generates primarily 2-hydroxylated E2, which is less toxic and has been considered as protective (Cavalieri et al., 2002; Liehr et al., 1995; Mobley et al., 1999; Schumacher et al., 1999; Yager and Liehr, 1996). Moreover, it has been suggested that the induction of mouse hepatic CYP1A1 is primarily protective for toxicity of DMBA (Uno et al., 2004). Therefore, it is possible that the prolongation of hepatic

CYP1B1 induction has been observed in the 250-ng group contributes to mammary carcinogenesis by bioactivation of both exogenous pro-carcinogens, DMBA, and endogenous E2.

A recent study showed elevated expression of AhR in the endometrium and myometrium (Khorram et al., 2002). In this study, the 250-ng group revealed elevated AhR expression compared to the other groups. Notably high levels of AhR in the liver of the 250-ng group suggest that elevated AhR expression mediated, at least in part, the increased expression of CYP1B1. As previously suggested, high levels of CYP1B1 expression, like hyperexpression of AhR, may represent a molecular marker for carcinogenesis (Spink et al., 1998). Moreover, AhR-deficient cells exhibit a decreased rate of cell proliferation because of a prolongation of cells in G1 (Ma and Whitlock, 1996; Weiss et al., 1996). The AhR also controls a number of genes whose products may be involved in a number of cellular proliferation and differentiation processes (Okey et al., 1994). In this study, because the 250-ng group showing enhancement of DMBA-induced mammary carcinogenesis revealed significantly higher AhR expression, AhR might mediate DMBA-induced mammary carcinogenesis through dysregulation of the cell cycle. However, it was unclear why a significantly lower induction of AhR was observed in the 7.5-μg group, which showed high-level PCB126 residues in mammary carcinomas, than in the 250-ng group.

Acknowledgments

The authors thank Ms. Katherine Ono for critical reading and editing of the manuscript. This study was supported by a Grant-in-Aid for High-Tech Research Center Project from the Ministry of Education, Science and Culture, Japan.

References

Angus, W.G., Larsen, M.C., Jefcoate, C.R., 1999. Expression of CYP1A1 and CYP1B1 depends on cell-specific factors in human breast cancer cell lines: role of estrogen receptor status. Carcinogenesis 20, 947–955.

Badawi, A.F., Cavalieri, E.I., Rogan, E.G., 2000. Effect of chlorinated hydrocarbons on expression of cytochrome P450 1A1, 1A2 and 1B1 and 2- and 4-hydroxylation of 17β-estradiol in female Sprague–Dawley rats. Carcinogenesis 21, 1593–1599.

Beleh, M.A., Lin, Y.C., Brueggemeier, R.W., 1995. Estrogen metabolism in microsomal, cell, and tissue preparations of kidney and liver from Syrian hamsters. J. Steroid Biochem. Mol. Biol. 52, 479–489.

Bolognesi, C., Parrini, M., Aiello, C., Rossi, L., 1991. DNA damage induced by 7,12-dimethylbenz[a]anthracene in the liver and the mammary gland of rats exposed to polycyclic aromatic hydrocarbon enzyme inducers during perinatal life. Mutagenesis 6, 113–116.

Bro-Rasmussen, F., 1996. Contamination by persistent chemicals in food chain and human health. Sci. Total Environ. 188, 45–60.

Burback, K.M., Poland, A.P., Bradifield, C.A., 1992. Cloning of the Ah receptor cDNA reveals a distinctive ligand-activated transcription factor. Proc. Natl. Acad. Sci. U.S.A. 89, 8185–8989.

Cavalieri, E.L., Balu, N., Saeed, M., Devanesan, P., 2002. Catechol ortho-quinones: the electrophilic compounds that form depurinating DNA adducts and could initiate cancer and other diseases. Carcinogenesis 23, 1071–1077.

Christou, M., Moore, C.J., Gould, M.N., Jefcoate, C.R., 1987. Induction of mammary cytochromes P-450: an essential first step in the metabolism of 7,12-dimethylbenz(*a*)anthracene by rat mammary epithelial cells. Carcinogenesis 8, 73–80.

Christou, M., Sava, U., Schroeder, S., Shen, X., Thompson, T., Gould, M., Jefcoate, C., 1995. Cytochromes CYP1A1 and CYP1B1 in the rat mammary gland: cell-specific expression and regulation by polycyclic aromatic hydrocarbons and hormones. Mol. Cell. Endocrinol. 115, 41–50.

Ciolino, H., Dankwah, M., Yeh, G., 2002. Resistance of MCF7 cells to dimethylbenz(*a*)anthracene induced apoptosis is due to reduced CYP1A1 expression. Int. J. Oncol. 21, 385–391.

Daniel, F.B., Joyce, N.J., 1984. 7,12-dimethylbenz[*a*]anthracene-DNA adduct in Sprague–Dawley and Long–Evans female rats. Carcinogenesis 5, 1021–1026.

Di Giovanni, J., Juchau, M.R., 1980. Biotransformation and bioactivation of 7,12-dimethylbenz[*a*]anthracene. Drug Metab. 11, 61–101.

Dipple, A., 1995. DNA adducts of chemical carcinogens. Carcinogenesis 16, 437–441.

Dipple, A., Moschel, R.C., Bigger, C.A.H., 1984. Polynuclear aromatic carcinogens. In: Earle, C.E.S. (Ed.), Chemical Carcinogens, 2nd ed. American Chemical Society, Washington, pp. 245–314.

Dipple, A., Khan, Q.A., Page, J.E., Ponten, I., Szeliga, J., 1999. DNA reactions, mutagenic action and stealth properties of polycyclic aromatic hydrocarbon carcinogenesis. Int. J. Oncol. 14, 103–111.

Dolwick, K.M., Schmidt, J.V., Carver, L.A., Swanson, H.J., Bradfield, C.A., 1993. Cloning and expression of a human Ah receptor cDNA. Mol. Pharmacol. 44, 911–917.

El-Bayoumy, K., Chae, Y.H., Upadhyaya, P., Meschter, C., Cohen, L.A., Reddy, B.S., 1992. Inhibition of 7,12-dimethylbenz[*a*]anthracene-induced tumors and DNA adduct formation in mammary glands of female Sprague–Dawley rats by the synthetic organoselenium compound, 1,4-phenylenebis[methylene]selenocyanate. Cancer Res. 52, 2402–2407.

Eltom, S., Larsen, M., Jefcoate, C., 1998. Expression of CYP1B1 but not CYP1A1 by primary cultured human mammary stromal fibroblasts constitutively and in response to dioxin exposure: role of the Ah receptor. Carcinogenesis 19, 1437–1444.

Evans, R.M., 1988. The steroid and thyroid hormone receptor superfamily. Science 240, 889–895.

Ginsberg, G.L., Atherholt, T.B., 1989. Transport of DNA-adducting metabolites in mouse serum following benzo(*a*)pryene administration. Carcinogenesis 10, 673–679.

Granberg, A.L., Brunstrom, B., Brandt, I., 2000. Cytochrome P450-dependent binding of 7,12-dimethylbenz[*a*]anthracene (DMBA) and benzo[*a*]pyrene (B[*a*]P) in murine heart, lung, and liver. Arch. Toxicol. 74, 593–601.

Heidel, S.M., Czuprynski, C.J., Jefcoate, C.R., 1998. Bone marrow stromal cells constitutively express high levels of cytochrome P4501B1 that metabolize 7,12 dimethlbenz[*a*]anthracene. Mol. Pharmacol. 54, 1000–1006.

Hoffman, E.C., Reyes, H., Chu, F.F., Sander, F., Conley, L.H., Brooks, B.A., Handkinson, O., 1991. Cloning of a factor required for activity of the Ah (dioxin) receptor. Science 252, 954–958.

Huggins, C., Grand, L.C., Brillantes, F.K., 1961. Mammary cancer induced by a single feeding of polynuclear hydrocarbons, and its suppression. Nature 189, 204–207.

IARC Working Group on the Evaluation of Carcinogenic Risks to Humans: Polychlorinated dibenzo-*para*-dioxins and polychlorinated dibenzofurans, 1997. IARC Monogr. Eval. Carcinog. Risks Hum. 69, 1–631.

Jones, P.B.C., Durrin, L.K., Galeazzi, D.R., Whilock, J., 1986. Control of cytochrome P-450 gene expression: analysis of a dioxin-responsive enhancer system. Proc. Natl. Acad. Sci. U.S.A. 83, 954–958.

Khorram, O., Gathwaite, M., Golos, T., 2002. Uterine and ovarian aryl

hydrocarbon receptor (AHR) and aryl hydrocarbon receptor nuclear translocator (ARNT) mRNA expression in benign and malignant gynecological conditions. Mol. Hum. Reprod. 8, 75–80.

Kothari, L., Subramanian, A., 1992. A possible modulatory influence of melatonin on representative phase I and II drug-metabolizing enzymes in 9,10-dimethyl-1,2-benzantracene-induced rat mammary tumorigenesis. Anti-Cancer Drugs 3, 623–928.

Kutz, F.W., Wood, P.H., Bottimore, D.P., 1991. Organochlorine pesticides and polychlorinated biphenyls in human adipose tissue. Rev. Environ. Contam. Toxiol. 60, 115–120.

Liehr, J.G., Ricci, M.J., Jefcoate, C.R., Hannigan, E.V., Hokanson, J.A., Zhu, B.T., 1995. 4-Hydroxylation of estradiol by human uterine myometrium and myoma microsomes: implications for the mechanism of uterine tumorigenesis. Proc. Natl. Acad. Sci. U.S.A. 92, 9220–9224.

Ma, Q., Whitlock, J.P., 1996. The aromatic hydrocarbon receptor modulates the Hepa 1c1c7 cell cycle and differentiated state independently of dioxin. Mol. Cell. Biol. 16, 2144–2150.

MacDonald, C.J., Cliolino, H.P., Yeh, G.C., 2001. Dibenzoylmethane modulates aryl hydrocarbon receptor function and expression of cytochromes P450 1A1 1B1. Cancer Res. 61, 3919–3924.

Merchant, M., Krishnan, V., Safe, S., 1993. Mechanism of action of alpha-naphthoflavone as an Ah receptor antagonist in MCF-7 human breast cancer cell. Toxicol. Appl. Pharmacol. 120, 53–63.

Mobley, J.A., Bhat, A.S., Bruggemeier, R.W., 1999. Measurement of oxidative DNA damage by catechol estrogens and analogues in vivo. Chem. Res. Toxicol. 12, 270–277.

Moon, C.J., Tricomi, W.A., Gould, M.N., 1988. Comparison of 7,12-dimethylbenz[*a*]anthracene metabolism and DNA binding in mammary epithelial cells from three rat strains with differing susceptibilities to mammary carcinogenesis. Carcinogenesis 9, 2099–2102.

Murphy, R., Harvey, C., 1985. Residues and metabolites of selected persistent halogenated hydrocarbons in blood samples from a general population survey. Environ. Health Perspect. 60, 115–130.

Murray, G.L., Taylor, M.C., McFadyen, M.C., MacKay, J.A., Greenlee, W.F., Burke, M.D., Melvin, W.T., 1997. Tumor-specific expression of cytochromes P450 CYP1B1. Cancer Res. 57, 3026–3031.

Muto, T., Wakui, S., Imano, N., Nakaaki, K., Hano, H., Furusato, M., Masaoka, T., 2001. In-utero and lactational exposure of 3,3′,4,4′,5-pentachlorobiphenyl modulate dimethylbenz[*a*]anthracene-induced rat mammary carcinogenesis. J. Toxicol. Pathol. 14, 213–224.

Muto, T., Watanabe, T., Moto, M., Okamura, M., Kashida, Y., Kanai, Y., Mitsumori, K., Endou, H., 2003. Time course of expression of 7,12-dimethylbenz[*a*]anthracene-induced CYP1A1 and CYP1B1 mRNA and protein in rat liver. J. Toxicol. Pathol. 16, 287–290.

Nandi, S., Guzman, R.C., Yang, J., 1995. Hormones and mammary carcinogenesis in mice, rat, and humans: a unifying hypothesis. Pro. Natl. Acad. Sci. U.S.A. 92, 3650–3657.

Okey, A.B., Riddick, D.S., Harper, P.A., 1994. The Ah receptor: mediator of the toxicity of 2,3,7,8-tetrachlorocibenzo-*p*-dioxin (TDCC) and related compounds. Toxicol. Lett. 70, 1–22.

Rogan, W.J., Gladen, B.C., McKinney, J.D., Carreras, N., Hardy, P., Thullen, J., Tigelstad, J., Tully, M., 1987. Polychlorinated biphenyls (PCBs) and dichlorodiphenyl dichloroethane (DDE) in human milk: effects on growth, morbidity and duration of lactation. Am. J. Publ. Health 77, 1294–1297.

Rowlands, J., He, L., Hakkak, R., Roins, M., Badger, T., 2001. Soy and whey proteins downregulate DMBA-induced liver and mammary gland CYP1 expression in female rats. Nutr. Cancer 131, 109–134.

Safe, S., Krishnan, V., 1995. Cellular and molecular biology of aryl hydrocarbon (Ah) receptor-mediated gene expression. Arch. Toxicol. 17, 99–115.

Sasaki, M., Kaneuchi, M., Fujimoto, S., Tanaka, Y., Dahiya, R., 2003. CYP1B1 gene in endometrial cancer. Mol. Cell. Endocrinol. 202, 171–176.

Schmidt, J., Bradfield, C., 1996. Ah receptor signaling pathways. Annu. Rev. Cell Dev. Biol. 12, 55–89.

Schumacher, G., Kataoka, M., Roth, J.A., Mukhopadhyay, T., 1999. Potent antitumor activity of 2-methoxyestradiol in human pancreatic cancer cell lines. Clin. Cancer Res. 5, 493–499.

Semin, B.K., Esakova, T.D., Petrusevich, I.M., Tarusov, B.N., 1976. Metabolism of 7,12-dimethylbenz(alpha)anthracene in vivo. Vopr. Onkol. 22, 54–58.

Shimada, T., Hayer, C., Yamazaki, H., Amin, S., Hecht, S., Guengerich, F., Sutte, T., 1996. Activity of chemically diverse precarinogens by human cytochrome P-450 1B1. Cancer Res. 56, 2979–2984.

Slaga, T.J., Gleason, G.L., DiGiovanni, J., Sukumaran, K.B., Harvey, R.G., 1979. Potent tumor-initiating activity of the 3,4-dihydrodiol of 7,12-dimethylbenz[*a*]anthracene in mouse skin. Cancer Res. 39, 1721–1723.

Slims, P., Grover, A., 1981. Involvement of dihydrodiols and dioepoxides in the metabolic activation of polycyclic hydrocarbons other than benzo[*a*]pyrene. In: Glboin, H.V., Ts'o, P.O.P. (Eds.), Polycyclic Hydrocarbons and Cancer, vol. 3. Academic Press, New York, NY, pp. 117–181.

Spink, D., Katz, B., Hussain, M., Pentecost, B., Cao, Z., Spink, C., 1998. Estrogen regulates Ah responsiveness in MCF-7 breast cancer cells. Carcinogenesis 24, 1941–1950.

Tanabe, S., Tatsukawa, R., Phillips, D., 1987. Mussels as bioindicators of PCB pollution: a case study on uptake and release of PCB isomers and congeners in green-lipped mussels (*Perna viridis*) in Hong Kong waters. Environ. Pollut. 47, 41–62.

Tritscher, A.M., Goldstein, J.A., Portier, C.J., McCoy, Z., Clark, G.C., Lucier, G.W., 1992. Dose-response relationships for chronic exposure to 2,3,7,8,-tetrachlorodibenzo-*p*-dioxin in a rat tumor promotion model: quantification and immunolocalization of CYP1A1 and CYP1A2 in the liver. Cancer Res. 52, 3436–3442.

Turteltaub, K.W., Felton, J.S., Gledhill, B.L., Vogel, J.S., Southon, J.R., Caffee, M.W., Finkel, R.C., Nelson, D.E., Procter, I.D., David, J.C., 1990. Accelerator mass spectrometry in biomedical dosimetry: relationship between low-level exposure and covalent binding of heterocyclic amine carcinogens to DNA. Proc. Natl. Acad. Sci. U.S.A. 87, 5288–5292.

Uno, S., Dalton, T.P., Derkenne, S., Curran, C.P., Miller, M.L., Shertzer, H.G., Nebert, D.W., 2004. Oral exposure to benzo[*a*]pyrene in the mouse: detoxication by inducible cytochrome P450 is more important than metabolic activation. Mol. Pharmacol. 65, 1225–1237.

van den Berg, M., Birnbaum, L., Bosveld, A.T.C., Brunstrom, B., Cook, P., Feely, M., Giesy, J.P., Hanberg, A., Hasegawa, R., Kennedy, S.W., Kubiak, T., Larsen, J.C., Rolaf van Leeuwen, F.X., Liem, A.K.D., Nolt, C., Peterson, R.E., Poellinger, L., Safe, S., Schrenk, D., Tillitt, D., Tysklind, M., Younes, M., Waern, F., Zacharewski, T., 1998. Toxic equivalency factors (TEFs) for PCBs, PCDDs, PCDFs for human and wildlife. Environ. Health Perspect. 106, 775–792.

Waalkes, M.P., Liu, J., Chen, H., Xie, Y., Achanzar, W.E., Zhou, Y.S., Cheng, M.L., Diwan, B.A., 2004. Estrogen signaling in livers of male mice with hepatocellular carcinoma induced by exposure to arsenic in utero. J. Natl. Cancer Inst. 96, 466–474.

Wang, M.Y., Liehr, J.G., 1994. Identification of fatty acid hydroperoxide cofactors in the cytochrome P450-mediated oxidation of estrogens to quinone metabolites. Role and balance of lipid peroxides during estrogen-induced carcinogenesis. J. Biol. Chem. 269, 284–291.

Weinberg, R.A., 1996. How cancer arises. Sci. Am. 275, 62–70.

Weiss, C., Kolluri, S.K., Kiefer, F., Gottlicher, M., 1996. Complementation of Ah receptor deficiency in hepatoma cells: negative feedback regulation and cell cycle control by Ah receptor. Ex. Cell Res. 226, 154–163.

Whitlock, J., 1999. Induction of cytochrome P4501A1. Annu. Rev. Pharmacol. Toxicol. 39, 103–125.

Yager, J.D., Liehr, J.G., 1996. Molecular mechanisms of estrogen carcinogenesis. Annu. Rev. Pharmacol. Toxicol. 36, 203–232.

Modulation of Renal Apical Organic Anion Transporter 4 Function by Two PDZ Domain–Containing Proteins

Hiroki Miyazaki,*† Naohiko Anzai,* Sophapun Ekaratanawong,* Takeshi Sakata,* Ho Jung Shin,* Promsuk Jutabha,* Taku Hirata,* Xin He,* Hiroshi Nonoguchi,† Kimio Tomita,† Yoshikatsu Kanai,* and Hitoshi Endou*

Department of Pharmacology and Toxicology, Kyorin University School of Medicine, Mitaka-shi, Tokyo, Japan; and †Department of Nephrology, Graduate School of Medical Sciences, Kumamoto University, Kumamoto-shi, Kumamoto, Japan

Human organic anion transporter 4 (OAT4) is an apical organic anion/dicarboxylate exchanger in the renal proximal tubules and mediates high-affinity transport of steroid sulfates such as estrone-3-sulfate (E_1S) and dehydroepiandrosterone sulfate. Here, two multivalent PDZ (PSD-95/Discs Large/ZO-1) proteins PDZK1 and NHERF1 were examined as interactors of OAT4 by a yeast two-hybrid assay. These interactions require the extreme C-terminal region of OAT4 and the first and fourth PDZ domains of PDZK1 and the first PDZ domain of NHERF1. These interactions were confirmed by surface plasmon resonance assays (K_D: 36 nM, 1.2 μM, and 41.7 μM, respectively). *In vitro* binding assays and co-immunoprecipitation studies revealed that the OAT4 wild-type but not a mutant lacking the PDZ motif interacted directly with both PDZK1 and NHERF1. OAT4, PDZK1, and NHERF1 proteins were shown to be localized at the apical membrane of renal proximal tubules. The association with PDZK1 or NHERF1 enhanced OAT4-mediated E_1S transport activities in HEK293 cells (1.2- to 1.4-fold), and the deletion of the OAT4 C-terminal PDZ motif abolished this effect. The augmentation of the transport activity was accompanied by alteration in V_{max} of E_1S transport *via* OAT4 and was associated with the increased surface expression level of OAT4 protein. This study indicates that the functional activity of OAT4 is modulated through the PDZ interaction with the network of PDZK1 and NHERF1 and suggests that OAT4 is involved in the regulated apical organic anion handling in the renal proximal tubules, provided by the PDZ scaffold.

J Am Soc Nephrol 16: 3498–3506, 2005. doi: 10.1681/ASN.2005030306

The human organic anion transporter OAT4 (encoded by *SLC22A11*) is expressed in the kidney and the placenta and mediates the high-affinity transport of steroid sulfates such as estrone-3-sulfate (E_1S) and dehydroepiandrosterone sulfate (DHEAS) (1). Because of its apical membrane localization in the renal proximal tubules (2), OAT4 had been presumed to be the apical exit pathway of organic anions that are taken up by the basolateral entrance pathway such as OAT1 and OAT3 (3). Recently, Ugele *et al.* (4) found the OAT4 protein expression at the fetal side of the syncytiotrophoblasts in the placenta and proposed a role for OAT4 in the placental uptake of fetal-derived steroid sulfates. On the basis of our finding that OAT4 is an apical organic anion/dicarboxylate exchanger (5), we suggested that OAT4 mainly functions as an apical entrance pathway for some organic anions in renal proximal tubules driven by an outwardly directed dicarboxylate gradient created by Na^+/dicarboxylate co-transporters (6). One possible role of OAT4 is as an apical backflux pathway (7) for some organic anions such as steroid sulfates, functionally coupled to the apical efflux transporters for organic anions, such as MRP2, MRP4, and NPT1 (putative human homologue of OAT_V1) (8–13).

At the extreme C-terminal (CT) end, OAT4 has a specific protein–protein interaction peptide sequence named the PDZ (PSD-95/Discs Large/ZO-1) motif (S-T-S-L) (14). PDZ domains have been identified in various proteins and are known to be modular protein–protein recognition domains that play roles in protein targeting and protein complex assembly (15–17). These multidomain molecules not only target and provide scaffolds for protein–protein interactions but also modulate the function of receptors and ion channels, by which they associate. Recently, we reported that the urate/anion exchanger URAT1 (18), which has a similar PDZ motif (S-T-Q-F) at its C-terminus, interacts with multivalent PDZ protein PDZK1 (19,20). In the same study, we also identified that PDZK1 interacted with the C-terminus of OAT4, which has a PDZ motif, but not with those of human OAT1, OAT2, or OAT3, which do not have PDZ motifs (20). Both URAT1 and OAT4 are considered to function to generate a reabsorptive pathway for organic anions localized at the apical membrane of renal proximal tubules. Therefore, it is likely that these transporters bind with the same or other PDZ protein(s) *via* their CT PDZ motifs.

Received March 22, 2005. Accepted September 1, 2005.

Published online ahead of print. Publication date available at www.jasn.org.

H.M. and N.A. contributed equally to this work.

Address correspondence to: Dr. Yoshikatsu Kanai, Department of Pharmacology and Toxicology, Kyorin University School of Medicine, 6-20-2 Shinkawa, Mitaka, Tokyo 181-8611, Japan. Phone: +81-422-47-5511; Fax: +81-422-79-1321; E-mail: ykanai@kyorin-u.ac.jp

ISSN: 1046-6673/1612-3498

In this study, we examined the interaction between OAT4 and two PDZ proteins, PDZK1 and NHERF1, using a yeast two-hybrid assay, an *in vitro* pulldown assay, co-immunoprecipitation, and surface plasmon resonance assay. We observed that the OAT4-mediated transport function is modulated equivalently by binding with two PDZ proteins *via* the C-terminus of OAT4. These results, together with recent emerging findings concerning PDZ proteins, will provide important insight into the renal apical handling of organic anions through the transporter complexes supported by PDZ protein networks.

Materials and Methods

Plasmid Construction

DNA encoding residues 513 to 550 (wt, T548A, L550A) or 513 to 547 (d3) of human OAT4 were amplified by PCR using specific primers (Table 1) and cloned into the EcoRI and XhoI sites of the pEG202 plasmid (bait) and into pGEX-6P-1 (Amersham Biosciences, Inc., Piscataway, NJ) to generate OAT4-CT-wt, OAT4-CT-d3, OAT4-L550A, or OAT4-T548A. The full-length coding sequence of human OAT4 (wt) as well as its CT-3-amino-acid deletion mutant (d3) were inserted into the mammalian expression plasmid pcDNA3.1 (Invitrogen, Gaithersburg, MD) for functional analysis and into the pEGFP-C2 plasmid (Clontech, Palo Alto, CA) for GFP-fused OAT4 protein preparation. Proper folding of GFP-fused proteins was confirmed by their significant transport activities of E_1S (data not shown). The full-length coding sequence of human NHERF1 was amplified from human kidney cDNA (Clontech) and subcloned into pcDNA3.1 (Invitrogen) to generate pcDNA3.1-NHERF1 and into pJG4–5, a B42 activation domain fusion vector, to generate pJG4–5-NHERF1. Prey vectors (pJG4–5) that contained the individual PDZ domains of human NHERF1 were generated by PCR using specific primers (Table 1). The pcDNA3.1 vector that contained the full-length human PDZK1 and prey vectors that contained a single PDZ domain of human PDZK1 were prepared as described previously (20).

Yeast Two-Hybrid Assay

Yeast two-hybrid assays were performed in the EGY48 strain with the LexA-based *GFP* two-hybrid system (Grow'n'Glow system; MoBiTec, Göttingen, Germany) as described elsewhere (21).

GST Fusion Protein Binding Assays

The OAT4-CT domains for GST fusion protein production in bacteria were prepared as reported previously (21). *In vitro* translation was performed from a plasmid carrying the full-length PDZK1 and NHERF1 with the TNT T7 Quick for PCR DNA system (Promega, Madison, WI) in the presence of Transcend Biotinylated tRNA (Promega), as described elsewhere (20). Five microliters of *in vitro*–translated products was applied into ProFound Pull-Down GST Protein: Protein Interaction Kit (Pierce, Rockford, IL) with 50 μl of GST-glutathione-Sepharose resin, and protein complexes were eluted according to the manufacturer's instructions.

Surface Plasmon Resonance

The interactions of OAT4-CT with the first and fourth PDZ domains of PDZK1 and the first PDZ domains of NHERF1 were investigated using a BIAcore 3000 analytical system (BIAcore AB, Uppsala, Sweden) based on principles described previously (22). Using an amine coupling kit, GST-fused OAT4-CT wild-type or GST protein alone was attached to a CM5 sensor chip according to the manufacturer's instructions, giving a gain of 13,269 resonance units (RU) for GST-OAT4-CT or 8566 RU for GST alone.

Tissue Distribution

Aliqouts of 1.5 μl of Human Multiple Tissue cDNA Panels I and II (Clontech) were amplified as described previously (20). The OAT4 and NHERF1 primers used for PCR amplification are shown in Table 1.

Immunohistochemical Analysis

We used human single-tissue slides (Biochain) for light microscopic immunohistochemical analysis, and they were treated with 10 μg/ml primary rabbit polyclonal antibodies against OAT4 and hPDZK1 and with EBP50 (NHERF1)-specific mAb purchased from BD Bioscience (San Jose, CA) (23) at 4°C overnight, as reported previously (5).

Cell culture and Transfections

Human embryonic kidney 293 (HEK293) cells were maintained in DMEM supplemented with 10% FBS, 1 mM sodium pyruvate, 100 units/ml penicillin, and 100 mg/ml streptomycin (Invitrogen) at 37°C and 5% CO_2. Transient transfection with Lipofectamine 2000 (Invitrogen) was performed according to the manufacturer's recommendations. For the establishment of OAT4-expressing cells, stable transfectants were selected for 2 wk by adding 1 mg/ml G418 to the medium.

Immunoprecipitation and Immunoblotting

Immunoprecipitation analysis was performed as described previously (20). GFP-fused OAT4 and associated proteins in HEK293 cell lysate were immunoprecipitated by the anti-GFP antibody (full-length A.v. polyclonal antibody; Clontech) using the Seize Classic (A) Immunoprecipitation kit (Pierce). The eluates were treated as described in the GST Fusion Protein Binding Assays section. The affinity-purified rabbit PDZK1 antibodies, EBP50 antibody (23), and horseradish peroxidase–conjugated goat anti-rabbit IgG (Amersham Biosciences, Inc.) were used for immunoblotting with enhanced chemiluminescence reagents (ECL Plus; Amersham Biosciences, Inc.).

Table 1. PCR primers used in this study

Construct	Sense Primer	Antisense Primer
OAT4-CT-wt	5′-TGAATTCGAGACCCAGGGACTTCC-3′	5′-CCCTCGAGTTTCTAGAGCGAGGTAC-3′
OAT4-CT-d3	5′-TGAATTCGAGACCCAGGGACTTCC-3′	5′-CCCTCGAGCTAACTTTCCACAGTGACGG-3′
OAT4-L550A	5′-TGAATTCGAGACCCAGGGACTTCC-3′	5′-CTCTCGAGCTAGGCCGAGGTACTTTCCACAG-3′
OAT4-T548A	5′-TGAATTCGAGACCCAGGGACTTCC-3′	5′-CCCTCGAGTTTCTAGAGCGAGGCACTTTCC-3′
NHERF1-PDZ1	5′-CACTCGAGATGAGCGCGGACGCAGC-3′	5′-TTCTCGAGTCACCGAAGCTCGCGCTGCTC-3′
NHERF1-PDZ2	5′-TTCTCGAGCTTCGGCCTCGGCTCTG-3′	5′-TGCTCGAGTCACTCGTCAGTTTCCCTGTC-3′
OAT4 RT-PCR	5′-TCTTGCTCAGTTTCCTTGGCC-3′	5′-GCTGTTGATTTCTGGCTCTCCA-3′
NHERF1 RT-PCR	5′-TTCTCGAGCTTCGGCCTCGGCTCTG-3′	5′-TGCTCGAGTCACTCGTCAGTTTCCCTGTC-3′

E_1S Transport Activity Assays

HEK293 cells, plated on 24-well culture plates at a density of 2×10^5 24 h before transfection, were incubated in Lipofectamine 2000 as described above. After 36 h, the culture medium was removed and the cells were incubated in serum-free Dulbecco's modified PBS (D-PBS; containing [in mM] 137 NaCl, 3 KCl, 8 Na_2HPO_4, 1 KH_2PO_4, 1 $CaCl_2$, and 0.5 $MgCl_2$ [pH 7.4]) supplemented with 5.5 mM D-glucose for 10 min. The uptake study was started by adding 500 μl of D-PBS that contained 50 nM [^{3}H]E_1S into the plate. After 2 min, the cells were washed twice in ice-cold D-PBS and lysed in 0.1 N NaOH for 20 min for scintillation counting.

For determining the kinetic parameters, the concentrations of E_1S were varied from 50 nM to 3000 nM. OAT4-mediated E_1S uptake was calculated as the difference between the values of uptake into HEK293 cells that stably expressed OAT4 (HEK-OAT4) and those of uptake into HEK293 cells that were transfected with vector only (HEK-mock). The kinetic parameters for the uptake *via* OAT4 were estimated using the following equation: $v = V_{max}[S]/(K_m + [S])$, where v is the uptake rate of substrates, [S] is the substrate concentration (μM) in the medium, and K_m is the Michaelis-Menten constant (μM). These values were determined using the Eadie-Hofstee equation.

Cell Surface Biotinylation

Surface biotinylation of OAT4 at the plasma membrane was performed as described elsewhere (20). Surface proteins in HEK-OAT4 cells that were transfected with pcDNA3.1(+)-hPDZK1, pcDNA3.1(+)-hNHERF1, or pcDNA3.1(+) empty vector were biotinylated with Sulfo-NHS-SS-Biotin (0.5 mg/ml; Pierce) in PBS for 30 min at 4°C. Cell lysates then were incubated with Ultralink-immobilized NeutrAvidin beads (Pierce) to precipitate biotinylated proteins. The bound proteins were eluted with SDS sample buffer and were subjected to SDS-PAGE and Western blotting followed by ECL (Amersham Biosciences). OAT4 was detected with affinity-purified polyclonal OAT4 antibody (1:5000) (5).

Statistical Analyses

Uptake experiments were conducted three times, and each uptake experiment was performed in triplicate. Values are presented as the means ± SEM. Statistical significance was determined by t test.

Results

Interaction between OAT4 and PDZK1/NHERF1 in a Yeast Two-Hybrid Assay

In our previous study, we reported that one of the OAT members, URAT1, binds to the multivalent PDZ domain protein PDZK1 (20). In parallel, we also identified that a bait vector that contains the OAT4 carboxyl-terminal tail (OAT4-CT) binds to PDZK1 using a yeast two-hybrid assay. Because the CT of OAT4 that has a PDZ motif (T-S-L) is different from the URAT1 CT (T-Q-F), this difference motivated us to extend the search for the interaction of OAT4 with other PDZ proteins expressed in the kidney, such as NHERF1/EBP50, NHERF2/E3KARP, and IKEPP (24,25). We observed the induction of two reporter genes (LEU and GFP) in the interaction of OAT4-CT with NHERF1 and NHERF2 and the induction of only one reporter gene (LEU) in the OAT4-CT and IKEPP interaction (data not shown). The specificities of these interactions were confirmed by the constructs with unrelated proteins. Because NHERF1 and PDZK1 but not NHERF2 are predominantly in the brush border (26), we focused our research on the interactions of OAT4-CT with both PDZK1 and NHERF1.

To identify the binding site of OAT4 that interacts with the two PDZ proteins, we constructed three mutant baits, as in our previous study (20). The first was a mutant that lacked the last three residues of OAT4, which play a crucial role in PDZ domain recognition (OAT4-CT-d3). In the second and third, the extreme CT leucine (0 position) or threonine (−2 position) of OAT4 were replaced by alanine (L550A and T548A), which was expected to abolish or strongly reduce the binding of PDZ proteins (14). All three mutant baits were unable to interact with PDZK1 full-length clone or the NHERF1 full-length clone (Table 2). Thus, these results suggested that OAT4 CT PDZ motif is the site responsible for interactions with PDZK1 and NHERF1.

Table 2. Specificity of PDZK1 and NHERF1 for interaction with the C-terminus of OAT4 in the yeast two-hybrid assay

	C-Terminal Residues (Last 10 Amino Acids)	PDZK1		NHERF1	
		LEU2	GFP	LEU2	GFP
OAT4-CT-wt	EAVTVESTSL*	+	+	+	+
OAT4-CT-d3	EAVTVES*	−	−	−	−
OAT4-L550A	EAVTVESTSA*	−	−	−	−
OAT4-T548A	EAVTVESASL*	−	−	−	−

	PDZK1				NHERF1	
	PDZ1	PDZ2	PDZ3	PDZ4	PDZ1	PDZ2
LEU2	+	−	−	+	+	−
GFP	+	−	−	+	+	−

[a]The system used for the yeast two-hybrid assay included the reporter genes LEU2 and GFP, which replaced the classical *lacZ* gene commonly used, and allowed fast and easy detection of positive clones with long-wave UV.